

GNE-781, A Highly Advanced Potent and Selective Bromodomain Inhibitor of Cyclic Adenosine Monophosphate Response Element Binding Protein, Binding Protein (CBP)

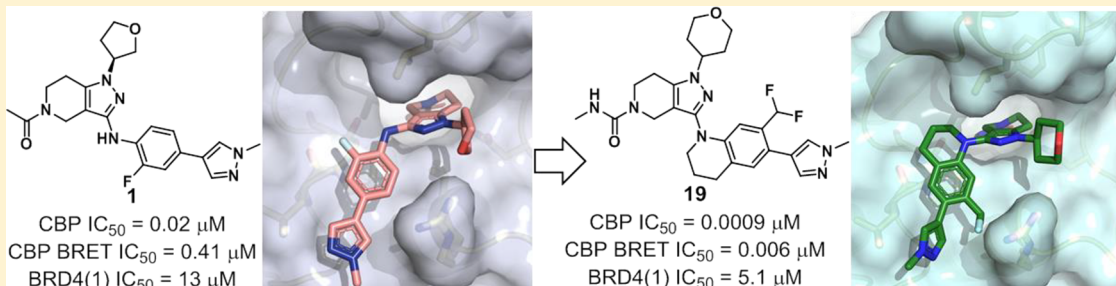
F. Anthony Romero,^{*†‡} Jeremy Murray,[†] Kwong Wah Lai,[‡] Vickie Tsui,[†] Brian K. Albrecht,[§] Le An,[†] Maureen H. Beresini,[†] Gladys de Leon Boenig,[†] Sarah M. Bronner,[†] Emily W. Chan,[†] Kevin X. Chen,[‡] Zhongguo Chen,[‡] Edna F. Choo,^{†‡} Kyle Clagg,[†] Kevin Clark,[†] Terry D. Crawford,^{†‡} Patrick Cyr,^{†‡} Denise de Almeida Nagata,[†] Karen E. Gascoigne,[†] Jane L. Grogan,[†] Georgia Hatzivassiliou,[†] Wei Huang,[‡] Thomas L. Hunsaker,[†] Susan Kaufman,[†] Stefan G. Koenig,^{†‡} Ruina Li,[†] Yingjie Li,[‡] Xiaorong Liang,[†] Jiangpeng Liao,[‡] Wenfeng Liu,[‡] Justin Ly,[†] Jonathan Maher,[†] Colin Masui,[†] Mark Merchant,[†] Yingqing Ran,[†] Alexander M. Taylor,[§] John Wai,[‡] Fei Wang,[‡] Xiaocang Wei,[‡] Dong Yu,[‡] Bing-Yan Zhu,[†] Xiaoyu Zhu,[‡] and Steven Magnuson^{*†‡}

[†]Genentech, Inc., 1 DNA Way, South San Francisco, California 94080, United States

[‡]Wuxi AppTec Co., Ltd., 288 Fute Zhong Road, Waigaoqiao Free Trade Zone, Shanghai 200131, People's Republic of China

[§]Constellation Pharmaceuticals, Inc., 215 First Street, Suite 200, Cambridge, Massachusetts 02142, United States

Supporting Information



ABSTRACT: Inhibition of the bromodomain of the transcriptional regulator CBP/P300 is an especially interesting new therapeutic approach in oncology. We recently disclosed in vivo chemical tool **1** (GNE-272) for the bromodomain of CBP that was moderately potent and selective over BRD4(1). In pursuit of a more potent and selective CBP inhibitor, we used structure-based design. Constraining the aniline of **1** into a tetrahydroquinoline motif maintained potency and increased selectivity 2-fold. Structure–activity relationship studies coupled with further structure-based design targeting the LPF shelf, BC loop, and KAc regions allowed us to significantly increase potency and selectivity, resulting in the identification of non-CNS penetrant **19** (GNE-781, TR-FRET IC₅₀ = 0.94 nM, BRET IC₅₀ = 6.2 nM; BRD4(1) IC₅₀ = 5100 nM) that maintained good in vivo PK properties in multiple species. Compound **19** displays antitumor activity in an AML tumor model and was also shown to decrease Foxp3 transcript levels in a dose dependent manner.

INTRODUCTION

The histone acetyl transferase (HAT) cAMP response element binding protein, binding protein (CREBBP, CBP), and highly homologous parologue, adenoviral E1A binding protein of 300 kDa (EP300, P300) are large, multidomain proteins that each contain a single bromodomain and contribute to transcriptional regulation.^{1–3} CBP/P300 (hereafter together referred to as “CBP”) bind to chromatin via their bromodomain. Once associated with chromatin, CBP modifies chromatin through its HAT activity, leading to the recruitment of various transcriptional proteins to modulate gene expression. CBP has been shown to bind nonhistone proteins and to recognize acetylated p53 at K382 following DNA damage.³ There have

been several studies that have implicated CBP in the development, maintenance, or progression of cancer and tumor immunity.^{4–8} Studies have shown that inhibition of the bromodomain of CBP regulates MYC⁹ (a regulator gene that plays a role in cell cycle progression and that is amplified in many cancers). Other studies have demonstrated that CBP bromodomain inhibition impairs differentiation of regulatory T cells (T_{reg}) and immunosuppressive function.¹⁰ To help understand the physiological implications of CBP in disease states, much work has centered around discovering novel chemical tools that

Received: June 5, 2017

Published: September 11, 2017



inhibit the bromodomain of CBP.^{11–19} These studies have revealed that inhibition of the CBP bromodomain is a promising new therapeutic approach in oncology and immuno-oncology.

We recently reported an *in vivo* chemical tool (**1**, GNE-272, Figure 1) as an inhibitor of the bromodomain of CBP that was

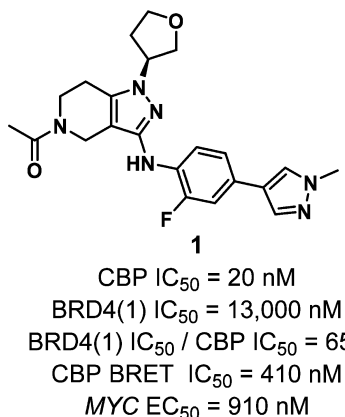


Figure 1. *In vivo* chemical tool **1** and potency data.

potent and 650-fold selective over the bromodomain **1** of the bromodomain-containing protein 4 [BRD4(1)] (BET bromodomain surrogate). We demonstrated through *in vivo* studies that **1** is able to modulate CBP MYC expression that corresponds with antitumor activity in a MYC-dependent acute myeloid leukemia (AML) model. While **1** is a promising *in vivo* tool to investigate CBP biology, we wished to extend our efforts to develop a more drug-like compound with improved cell potency and increased bromodomain selectivity, particularly over the bromodomain and extraterminal (BET) family.²⁰ Here we describe the design of **19** (GNE-781; 3-[7-(difluoromethyl)-6-(1-methylpyrazol-4-yl)-3,4-dihydro-2H-quinolin-1-yl]-N-methyl-1-tetrahydropyran-4-yl-6,7-dihydro-4H-pyrazolo[4,3-c]pyridine-5-carboxamide), a highly potent and selective CBP inhibitor that is efficacious in a MOLM-16 AML xenograft model. Additionally, *in vitro* studies show that **19** reduces FOXP3 (forkhead box P3) transcript levels, confirming earlier studies,¹⁰ with a less optimal chemical probe and suggesting that inhibition of the CBP bromodomain may provide a novel small molecule therapeutic approach for cancer immunotherapy.

RESULTS AND DISCUSSION

Co-crystal structures of **1** bound to both CBP and BRD4(1) provided insight toward understanding the selectivity preference of this compound for CBP over BRD4(1) (Figure 2).¹² Previously, we have shown that **1** binds to CBP and BRD4(1) in different conformations.¹² While **1** binds in a lower energy conformation in CBP, this compound binds at a higher energy conformation in BRD4(1) due to a residue difference in the WPF motif: Trp81, Pro82, and Phe83 for BRD4(1), and Leu1109, Pro1110, and Phe1111 for CBP (Figure 2).²¹ Upon binding to BRD4(1), the fluorophenylpyrazole arm of **1** is pushed into a strained conformation in-plane with the pyrazolopiperidine core to avoid clashing with Trp81.¹² With this in mind, we hypothesized that selectivity could be increased further on this scaffold by constraining the aniline nitrogen of **1** in a bicyclic, thus limiting the ability of the fluorophenylpyrazole to become coplanar with the pyrazolopiperidine core in the BRD4(1) binding site. Accordingly, we explored three saturated ring-size analogues (5-, 6-, or 7-membered) of **1** (Table 1). While indoline

Table 1. Constrained Analogs of **1**

compd	n	CBP IC ₅₀ (nM) ^a	BRD4(1) IC ₅₀ (nM) ^a	fold selectivity ^b
2	1	31	12000	387
3	2	16	20000	1250
4	3	1800	>20000	>11

^aAll IC₅₀ values are reported as the geometric mean from at least two determinations. TR-FRET assay with the isolated CBP or BRD4(1) bromodomain. ^bFold selectivity is defined by [BRD4(1) IC₅₀ (nM)/CBP IC₅₀ (nM)]

2 had a slight decrease in CBP potency and selectivity compared to parent **1**, tetrahydroquinoline (THQ) **3** maintained CBP potency and improved selectivity by nearly 2-fold. Expanding the ring further to a 7-membered ring (**4**) resulted in a significant loss

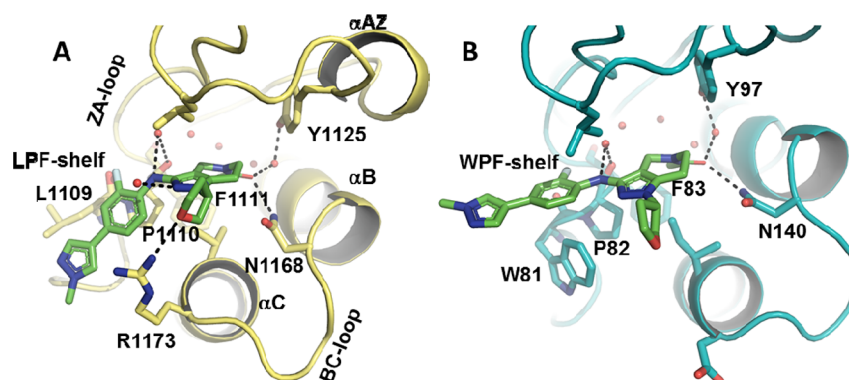


Figure 2. (A) A co-crystal structure of **1** (green) in the CBP bromodomain (yellow, 1.23 Å resolution, PDB SKTX) highlighting hydrogen bond interactions between the ligand and receptor. Water molecules are shown as small red spheres. (B) A co-crystal structure of **1** (green) and BRD4(1) (cyan, 1.14 Å resolution, PDB SKU3), highlighting hydrogen bond interactions between the ligand and receptor. Water molecules are shown as small red spheres.

in CBP potency, indicating the preferred conformations of the 7-membered ring are not accommodated in the binding site of CBP. We therefore used **3** as a template from which to further improve potency and selectivity. Because inhibition of the BET family bromodomains produces profound phenotypes, we were particularly focused on selectivity over BRD4(1) (our surrogate for BET bromodomains).

We obtained a co-crystal structure of **3** with the bromodomain of CBP (Figure 3). As observed with **1**, the amide of **3** binds in

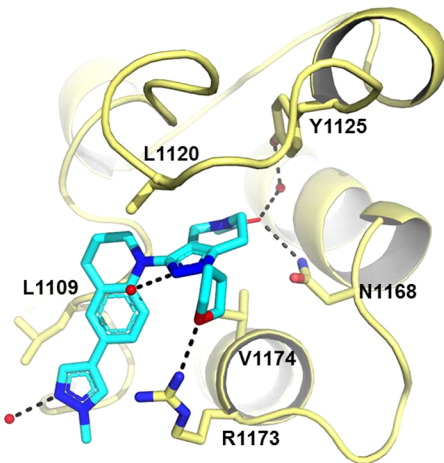
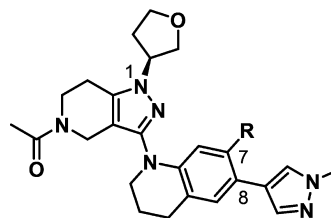


Figure 3. A co-crystal structure of **3** in the CBP (cyan) bromodomain (yellow, 1.6 Å resolution, PDB 5W0F) displaying important contacts between the ligand and receptor. Water molecules are shown as small red spheres.

the acetylated lysine (KAc) binding site, with the amide carbonyl making a canonical hydrogen bond to Asn1168 and additional water-mediated hydrogen bond interactions to Tyr1125. The pyrazolopiperidine core is sandwiched between the gatekeeper (Val1174) and Leu1120. The THQ ring makes van der Waals interactions with Pro1110 and Leu1120. The *N*-methylpyrazole packs along the lipophilic surface defined by the LPF shelf (Leu1109, Pro1110, Phe1111). Examination of the 3-CBP co-crystal structure revealed several areas in the binding site that could be explored to potentially improve potency. Initially, we examined structure–activity relationships (SAR) targeting Arg1173, the BC loop, and the KAc binding pocket.

We sought to improve the affinity of **3** by making favorable interactions with residues in the LPF shelf and Arg1173 through the introduction of various substituents to the 7-position of the THQ ring (Table 2).²² To explore potential hydrophobic interactions with the methylene side chain of Arg1173 and to test the feasibility of disrupting the planarity between the *N*-methyl pyrazole and the phenyl ring of the THQ methyl (**5**), chloro (**6**), and methoxy (**7**) substitutions were evaluated, resulting in each case in a 3.4–3.7-fold increase in CBP potency. The selectivity of **5** and **6** for CBP over BRD4(1) was comparable to parent **3**, while **7** had reduced (~3-fold) selectivity for CBP. To further increase van der Waals interactions with residues in the LPF shelf and potentially interact with the guanidine atoms of Arg1173, fluorine atoms were added to the 7-methyl of **5**. Notably, difluoro **8** demonstrated an 11-fold increase in CBP inhibitory potency compared to **3** and exhibited selectivity (BRD4/CBP) substantially exceeding that of **3**. Additionally, **8** had significantly improved cell potency (CBP BRET IC₅₀ = 37 nM). Trifluoro analogue **9** was also quite potent but had lower selectivity compared to **8**. While **9** was potentially an interesting compound

Table 2. Substitution at the 7-Position of the THQ



compd	R	CBP IC ₅₀ (nM) ^a	BRD4(1) IC ₅₀ (nM) ^a	CBP BRET IC ₅₀ (nM) ^b	fold selectivity ^c
3	H	16	20000	320	1250
5	CH ₃	4.4	7300	120	1659
6	Cl	4.3	4800	68	1116
7	OCH ₃	4.7	2200	140	468
8	CF ₂ H	1.4	5600	37	4000
9	CF ₃	1.5	4400	39	2933

^aAll IC₅₀ values are reported as the geometric mean from at least two determinations. ^bBRET assay in HEK293 cells transiently transfected with CBP-Nanoluc and histone H3.3-Halo tag constructs. ^cFold selectivity is defined by [BRD4(1) IC₅₀ (nM)/CBP IC₅₀ (nM)].

itself to follow up, we chose **8** to further examine SAR because it had a more favorable lipophilic ligand efficiency (cLogP²³ = 2.1; LLE²⁴ = 6.9) compared to **9** (cLogP = 3.6; LLE = 5.4). To further understand the increased CBP potency of **8**, we obtained a co-crystal structure of **8** and the CBP bromodomain (Figure 4). The crystal structure revealed that while **8** had a similar binding mode compared to **3**, additional favorable dipolar interactions between the partial negative charge on the fluorines of the 7-difluoromethyl and the positively charged guanidine on Arg1173 were observed. Relative to **3**, the *N*-methylpyrazole is rotated and lies out of plane by ~30°, as expected due to the CF₂H substitution (see Supporting Information for torsion scan plot). As a result, the *N*-methylpyrazole sits in a shallow crevice on the surface of CBP that is formed by the side chains of Leu1109, Val1174, and Phe1177 of the LPF shelf and the Cβ of Arg1173.

Further inspection of the co-crystal structure of **8** and CBP suggested that we could explore N1-substitution of the pyrazolopiperidine might increase hydrophobic interactions with residues in the BC and ZA loops. Figure 4B displays the surface of the protein around the THF moiety of **8** and indicates that expanding the THF to a 6-membered ring could increase van der Waals interactions with Leu1120 and Ile1122. Tetrahydropyran (THP) **10** resulted in an increase in both biochemical and cell potency (Table 3; it should be noted that the effective lower limit of the CBP TR-FRET assay is 1 nM, as the CBP concentration is 2 nM). Additionally, the stability of **10** in liver microsomes (LM) increased compared to **8**. A co-crystal structure of **10** with CBP shows similar interactions to those described for **3** and **8** with the exception of the THP ring (Figure 5). Rather than pointing toward Arg1173 as observed with the THF moiety, the oxygen atom of the THP pointed out toward solvent in the BC loop region and suggested that this region would enable us to tune physicochemical properties. To reduce the cLogP²³ of **10**, we investigated the addition of polar substituents to this area of the binding site. The structure suggested that these modifications would have minimal effect on the biochemical potency and potentially would increase LM stability. Removing the oxygen atom of the THP ring of **10** afforded cyclohexane **11** that had decreased CBP inhibitory potency. To further investigate polar atoms in this area, the

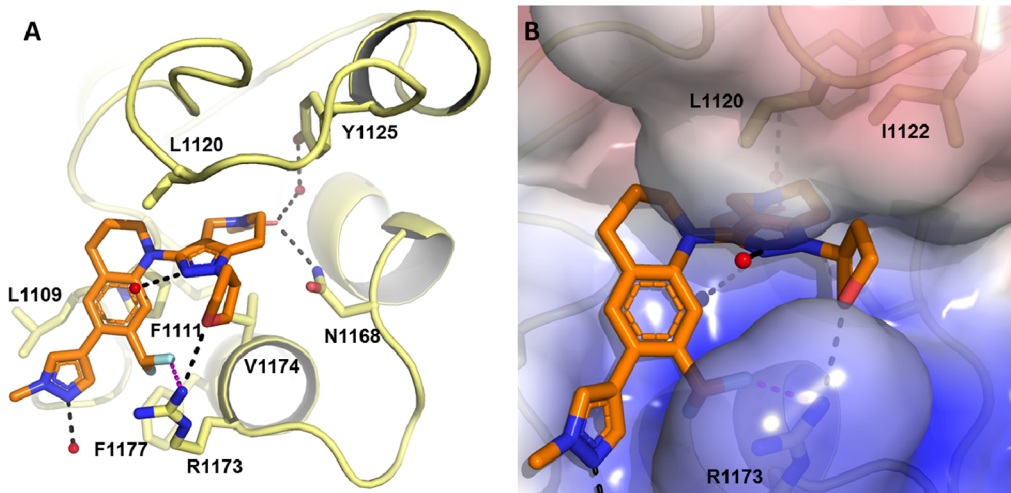


Figure 4. (A) Co-crystal structure of 8 (orange) in the CBP bromodomain (yellow, 1.43 Å resolution, PDB 5W0I) displaying important contacts between the ligand and receptor. Water molecules are shown as small red spheres. (B) The solvent accessible surface of the CBP bromodomain colored to highlight hydrophobicity and charge where hydrocarbon groups are white, atoms with a partial negative charge are red, and atoms with partial positive charge are blue. Bound ligand 8 is shown in stick representation (orange). Water molecules are shown as small red spheres.

Table 3. Exploration of SAR in the BC Loop Region of CBP

Cmpd	R	CBP ^a IC ₅₀ (nM)	BRD4(1) ^a IC ₅₀ (nM)	CBP BRET ^a IC ₅₀ (nM)	Fold Selectivity ^b	LM Cl _{hep} ^c M / R / H	cLogP
8		1.4	5,600	37	4,000	55 / 24 / 13	2.1
10		1.1	4,200	12	3,820	29 / 21 / 9.4	2.5
11		3.1	9,500	45	3,070	62 / 45 / 19	4.0
12		1.5	3,100	690	2,070	<18 / <7.7 / <4.8	2.2
13		2.0	4,200	98	2,100	54 / 22 / 17	2.8
14		1.0	4,100	53	4,100	39 / <6.1 / 10	2.1
15		1.2	4,000	46	3,300	25 / 23 / 6.2	1.7
16		1.2	5,400	41	4500	31 / 18 / 5.3	0.99

^aAll IC₅₀ values are reported as the geometric mean from at least two determinations. ^bFold selectivity is defined by [BRD4(1) IC₅₀ (nM)/CBP IC₅₀ (nM)]. ^cMouse (M), rat (R), and human (H) liver microsome-predicted hepatic clearance (mL/min/kg).

oxygen atom of **10** was replaced with a nitrogen to make piperidines **12** and **13**. While the biochemical potency of **12** only decreased slightly compared to **10**, there was a significant decrease in cell potency presumably that may indicate poor permeability of this compound. The N-methyl piperidine **13**

rescues the cell potency of **12** but leads to increased cLogP. The decrease in LM stability observed for **13** may be attributed to the increased cLogP. To lower cLogP and increase LM stability, we evaluated analogues **14**, **15**, and **16**. This afforded compounds with reduced cellular potency compared to **10** but limited

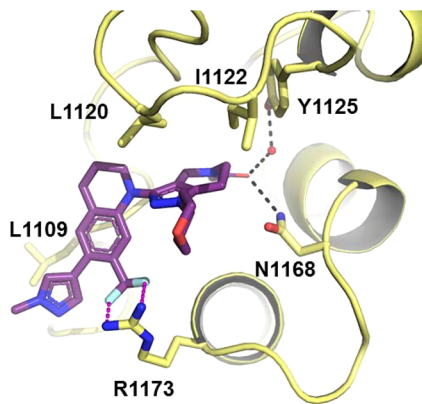


Figure 5. (A) Co-crystal structure of **10** (purple) in the CBP bromodomain (yellow, 1.55 Å resolution, PDB 5W0L) displaying important contacts between the ligand and receptor. Water molecules are shown as small red spheres.

increase in LM stability. Ultimately, **10** (GNE-049) was selected for further profiling as it had the best balance of LM stability, selectivity, and cellular potency (Figure 6). Furthermore, **10** demonstrated acceptable PK in mouse, rat, dog, and monkey. Determination of potency versus a selection of bromodomains revealed that this compound is selective for CBP/P300 (full bromodomain selectivity profile provided in Supporting Information) and, importantly, quite selective (3820-fold) over BRD4(1). The compound had excellent potency in the BRET

cellular assay and, in an orthogonal measure of the target engagement, **10** was shown to inhibit the expression of MYC⁹ (MV4-11 cell line) with an EC₅₀ of 14 nM. Compound **10** was further evaluated in a rat single dose (30–250 mg/kg QD) toxicokinetic study (data not shown). Adverse central nervous system (CNS)-related signs (e.g., marked hyperactivity and vocalization) were observed in several of the rats at the 250 mg/kg dose level. Furthermore, at the 250 mg/kg dose level, the ratio of the unbound drug concentration in brain to unbound drug concentration in plasma ($K_{p,uu}$) 3 h post dose was determined to be 0.43, indicating that compound was penetrating into the CNS and potentially resulting in the observed toxicity.

In pursuit of a more drug-like CBP inhibitor, we sought a compound with a similar profile to **10** but with limited CNS penetration. To do this, we targeted a molecule with increased total polar surface area (tPSA) (**10** tPSA = 68) and containing an additional H-bond donor. Previously, as part of our screening efforts, we had run a high-concentration fragment screen attempting to find alternative and novel Asn1168 binding chemotypes (not shown) and identified a highly ligand efficient²³ fragment, **17** (CBP IC₅₀ = 18 μM, LE = 0.41), that displayed >6-fold selectivity for CBP over BRD4 (Figure 7A). A co-crystal structure of this compound bound to the CBP bromodomain (Figure 7B) revealed the methyl urea moiety to be occupying the KAc binding pocket. The NH of the urea makes a hydrogen bond with the backbone of Pro1110, with the methyl group of the urea making van der Waals interactions with Phe1111. Interestingly, the phenyl ring of Phe1111 is rotated slightly such that the Cδ1

CBP IC ₅₀ (nM) ^a	P300 IC ₅₀ (nM) ^a	CBP BRET IC ₅₀ (nM) ^a	Myc EC ₅₀ (nM) ^a
1.1	1.3	12	14

In vitro stability & binding

Papp (A to B) ^b	PPB (%) ^c M/R/D/C/H	LM Cl _{hep} ^d M/R/D/C/H	Hep Cl _{hep} ^e M/R/D/C/H
15	92/88/81/79/84	32/21/16/22/10	<21/15/<7.8/<8.8/<6.2

PK Parameters

Species	CL (mL/min/kg)	t _{1/2} (h)	F (%)	V _{ss} (L/kg)	C _{max} (μM)	AUC _{last} (hr*μM)
Mouse ^f	8.8	1.1	72	0.81	4.2	13.7
Rat ^f	16	0.66	93	0.81	3.2	9.4
Dog ^g	4.6	4.2	94	1.0	5.1	31
Cyno ^g	7.4	2.8	39	1.4	1.6	8.5

Selectivity

Bromodomain	IC ₅₀ (nM) ^a
BAZ2B	>20,000
BPTF	>20,000
BRD4(1)	4,200
BRD4(2)	>20,000
BRD8(1)	>20,000
BRD9	>20,000
BRPF1	>20,000
CECR2	14,000
GCN5L	>20,000
PCAF	>20,000
TAF1(1)	>20,000
TAF1(2)	>20,000

cLogP: 2.5
Kinetic Solubility: 76 μM

Figure 6. Summary of potency, selectivity, and DMPK properties of **10**. ^aAll IC₅₀ values are reported as the geometric mean from at least two determinations. ^bMDCK cell line: apical-to-basolateral; units = $\times 10^{-6}$ cm s⁻¹. ^cMouse (M), rat (R), dog (D), cynomolgus monkey (C), and human (H) plasma protein binding. ^dLiver microsome-predicted hepatic clearance (mL/min/kg). ^eHepatocyte-predicted hepatic clearance (mL/min/kg). ^fCompound was dosed iv (1 mg/kg) as PEG400/H₂O (35/65) solution and po (5 mg/kg) as an aqueous suspension with 0.5% methylcellulose and 0.2% Tween 80. ^gCompound was dosed iv (1 mg/kg) as EtOH/PEG400/H₂O (20/15/65) solution and po (5 mg/kg) as an aqueous suspension with 0.5% methylcellulose and 0.2% Tween 80.

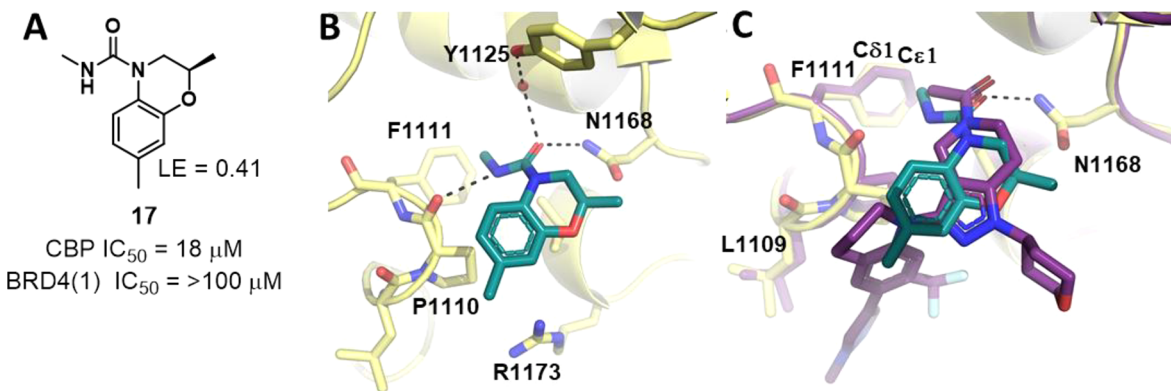
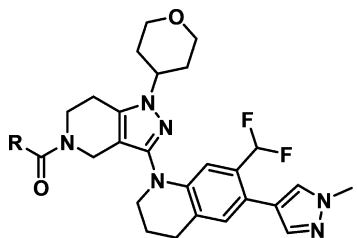


Figure 7. (A) CBP-selective fragment screening hit **17**. (B) Co-crystal structure of **17** (aqua) and the CBP bromodomain (yellow, 1.7 Å resolution; PDB SW0Q). Residues engaging in important contacts between the ligand and receptor are shown in stick representation. Water molecules are shown as small red spheres. (C) Compound **17** (aqua) overlaid with **10** (purple) in the CBP binding site (yellow).

and Cε1 atoms are 0.8 and 0.9 Å from their positions when bound to **10** (Figure 7C). From the structure of **10** overlaid with **17**, it appeared that the key Asn-binding acetamide of **10** could be replaced with a urea moiety. We therefore explored a small set of substituted urea analogues of **10** (Table 4). Primary urea **18**

Table 4. Exploring the KAc Binding Site with Urea Substitution



compd	R	CBP ^a IC ₅₀ (nM)	BRD4(1) ^a IC ₅₀ (nM)	BRET ^a IC ₅₀ (nM)	fold selectivity ^b
10	CH ₃	1.1	4200	12	3818
18	NH ₂	1	9600	28	8727
19	NHCH ₃	0.94	5100	6.2	5425
20	NHCH ₂ CH ₃	31	>20000	530	>645
21	N(CH ₃) ₂	310	15000	3700	48

^aAll IC₅₀ values are reported as the geometric mean from at least two determinations. ^bFold selectivity is defined by [BRD4(1) IC₅₀ (nM)]/[CBP IC₅₀ (nM)].

matched the biochemical potency of **10** and displayed a remarkable 9600-fold selectivity for CBP over BRD4(1). Methyl urea **19**, the same group present in fragment hit **17**, afforded subnanomolar biochemical potency, 5425-fold selectivity for CBP over BRD4(1), and <10 nM cellular potency. To further probe the KAc pocket, we made ethyl urea **20** and N,N-dimethyl urea **21**, but these resulted in 33-fold and 330-fold losses in potency, respectively, compared to **19**. The significant loss in potency observed with **21** was expected because it was assumed that the NH of the urea was participating in a H-bond with the backbone of Pro1110 similar to that observed with the **17**-CBP crystal structure.

To further understand the selectivity of **19**, we obtained co-crystal structures of this compound with CBP and BRD4(1) (Figure 8). In the **19**-CBP co-crystal structure, similar interactions with the binding site are observed as seen in the

10-CBP co-crystal crystal structure, with an additional interaction provided by the methyl urea of **19** (Figure 8A). As observed in the **17**-CBP co-crystal structure, the urea NH of **19** makes a hydrogen bond with the backbone of Pro1110 and the methyl group of the urea makes van der Waals interactions with Phe1111. Unsurprisingly, the Cδ1 and Cε1 atoms of Phe1111 shifted by 0.8 and 1.0 Å, respectively, relative to the **10** structure, consistent with the shifts observed in the **17**-CBP co-crystal structure. In BRD4, Trp81 from the WPF shelf served as a lipophilic “protrusion” compared to CBP’s LPF “wall” (Figure 8B). As a result, the THQ of **19** is rotated in BRD4(1) such that the phenyl ring makes van der Waals contacts with Leu92 from the BC loop while the N-methylpyrazole is completely solvent-exposed. The ligand–receptor complementarity of **19** in BRD4 is less optimal relative to **19** bound to CBP, providing an explanation for the selectivity.

On the basis of the cell potency and selectivity of **19**, we further profiled this compound (Figure 9). Compound **19** showed moderate to low clearance in vivo in all species evaluated, with acceptable oral bioavailability. Examination of a subset of bromodomains revealed that this compound is exquisitely selective for CBP/P300 (full bromodomain selectivity profile provided in Supporting Information) and is remarkably selective for CBP (5425-fold) and P300 (4250-fold). When tested (full details in Supporting Information) in an Invitrogen kinase panel (1 μM, 220 kinases), **19** did not inhibit any target at >10%, and in a Cerep off-target screening panel (10 μM, 43 receptors), **19** did not inhibit any target at >39%. In addition, **19** did not inhibit (>10 μM, top concentration) several cytochrome P450s (3A4, 1A2, 2C9, 2C19, 2D6). The compound had excellent and comparable potency (<10 nM) between the BRET and MYC cellular assays. Furthermore, when **19** was dosed in a rat at 250 mg/kg, the K_{p,uu} (3 h post dose) was determined to be 0.02 (compared to 0.43 for **10**), indicating that there was little brain penetration of this compound, and no adverse CNS-related signs were observed.

We next determined the effect of **19** in an in vivo PK/PD experiment using a MOLM-16 (adult AML cell line) xenograft mouse model. Single doses of **19** were given at dose levels between 3 and 30 mg/kg in MOLM-16 tumor-bearing animals, and samples were collected at time points covering 2–24 h. Tumor RNA was generated and used to assess MYC transcript by quantitative RT-PCR relative to vehicle-treated animals. Suppression of MYC was observed at doses as low as 3 mg/kg at 2 and 8 h, with maximal suppression observed at 10 and 30

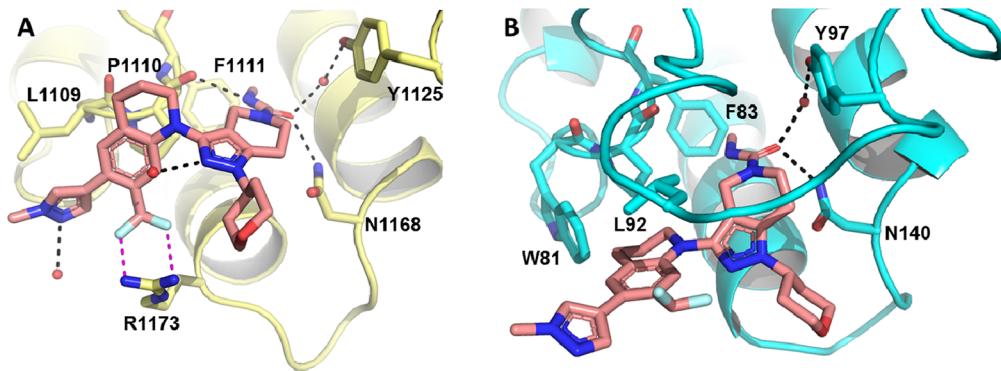


Figure 8. (A) Co-crystal structure of **19** (pink) and the CBP bromodomain (yellow, 1.41 Å resolution; PDB 5W0E). Residues engaging in important contacts between the ligand and receptor are shown in stick representation. Water molecules are shown as small red spheres. (B) Co-crystal structure of **19** (pink) and the BRD4(1) bromodomain (cyan, 1.71 Å resolution; PDB 5VZS). Residues engaging in important contacts between the ligand and receptor are shown in stick representation. Water molecules are shown as small red spheres.

				Selectivity		
CBP	P300	CBP BRET	Myc	Bromodomain	IC ₅₀ (nM) ^a	
IC ₅₀ (nM) ^a	IC ₅₀ (nM) ^a	IC ₅₀ (nM) ^a	EC ₅₀ (nM) ^a			
0.94	1.2	6.2	6.6			
<i>In vitro</i> stability & binding						
Papp (A to B) ^b	PPB (%) ^c M/R/D/C/H	LM Cl _{hep} ^d M/R/D/C/H	Hep Cl _{hep} ^e M/R/D/C/H			
19	94/94/77/78/84	35/18/17/23/10	<21/<10/<7.8/24/<6.2			
PK Parameters						
Species	CL (mL/min/kg)	t _{1/2} (h)	F (%)	V _{ss} (L/kg)	C _{max} (μM)	AUC _{last} (hr*μM)
Mouse ^f	5.2	1.4	73	0.60	23	6.5
Rat ^f	3.8	3.7	37	0.64	4.1	16
Dog ^g	4.8	4.7	100	1.5	8.3	44
Cyno ^g	18	0.72	28	1.0	1.9	2.5

cLogP: 2.4
Kinetic Solubility: 95 μM

Figure 9. Summary of potency, selectivity, and DMPK properties of **19**. ^aAll IC₅₀ values are reported as the geometric mean from at least two determinations. ^bMDCK cell line: apical-to-basolateral; units = $\times 10^{-6}$ cm s⁻¹. ^cMouse (M), rat (R), dog (D), cynomolgus monkey (C), and human (H) plasma protein binding. ^dLiver microsome-predicted hepatic clearance (mL/min/kg). ^eHepatic clearance (mL/min/kg). ^fCompound was dosed iv (1 mg/kg) as PEG400/H₂O (35/65) solution and po (5 mg/kg) as an aqueous suspension with 0.5% methylcellulose and 0.2% Tween 80. ^gCompound was dosed iv (1 mg/kg) as EtOH/PEG400/H₂O (20/15/65) solution and po (5 mg/kg) as an aqueous suspension with 0.5% methylcellulose and 0.2% Tween 80.

mg/kg at 2 h (87% and 88% inhibition, respectively; Figure 10A). It should be noted that suppression of MYC at the 3, 10, and 30 mg/kg doses was seen without tumor or plasma levels of **19** reaching the BRD4(1) IC₅₀ (5.1 μM), and thus results observed are clearly not from BET inhibition. Consistent with previous results,¹² inhibition of MYC-transcript was transient over the 24 h window with an apparent rebound effect at the 3 mg/kg dose level, rising to about 150% of vehicle control at the 16 h time point. Increasing suppression of MYC transcript level correlated with increasing plasma and tumor drug levels (Figure 10A).

To evaluate the in vivo efficacy of **19**, MOLM-16 AML xenografts were established in SCID beige mice. Upon tumor establishment, dosing of compound **19** was initiated with po doses of 3–30 mg/kg, twice daily (BID). Single-agent efficacy was observed at all doses, as evidenced by inhibition of MOLM-16 tumor growth (Figure 10B). Tumor growth inhibition (% TGI) was 73%, 71%, and 89% at 3, 10, and 30 mg/kg, respectively. All doses of **19** were well tolerated over the 21-day dosing window, with a maximal body weight loss of 3.7%. There was a lack of dose proportionality observed between the 3 and 10

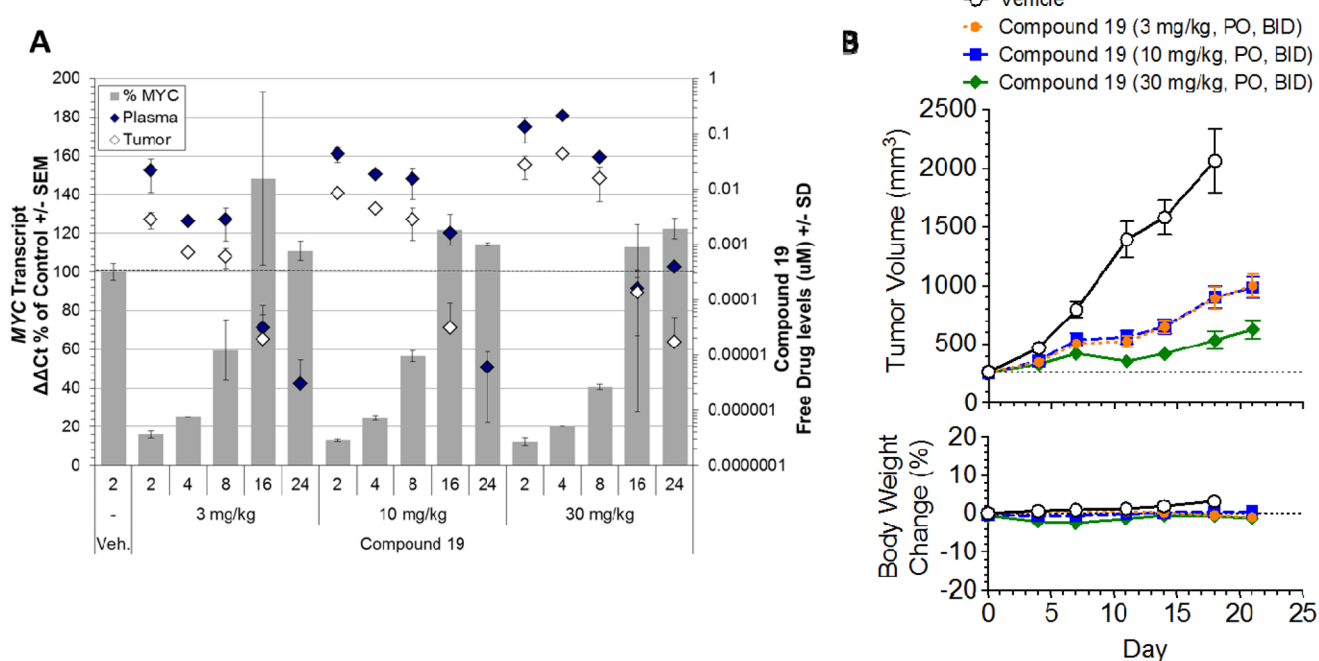


Figure 10. In vivo evaluation of **19**. (A) Effect on **19** treatment on *MYC* transcript levels in MOLM-16 xenograft tumors with single doses of **19** ($n = 3$ /group; mean \pm SEM plotted). Plasma and tumor levels were adjusted for PPB and tissue binding, respectively, and mean plasma and tumor unbound drug levels (\pm SD) are displayed. (B) Antitumor efficacy of **19** at 3, 10, and 30 mg/kg in the MOLM-16 AML xenograft tumor model and effect on body weight ($n = 10$ /group; tumor volume, mean \pm SEM plotted; body weight, group fitted % body weight loss plotted).

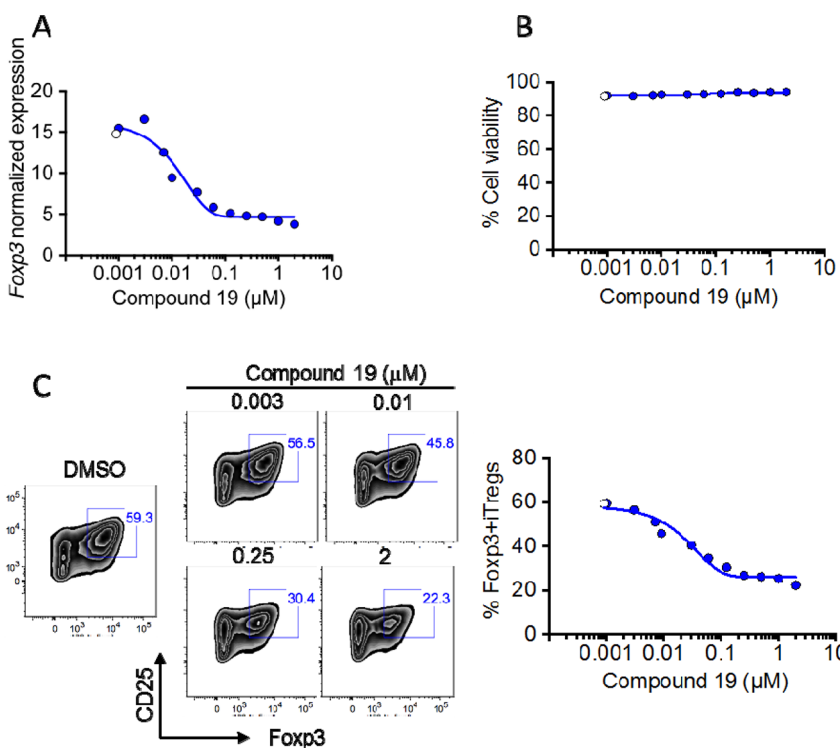
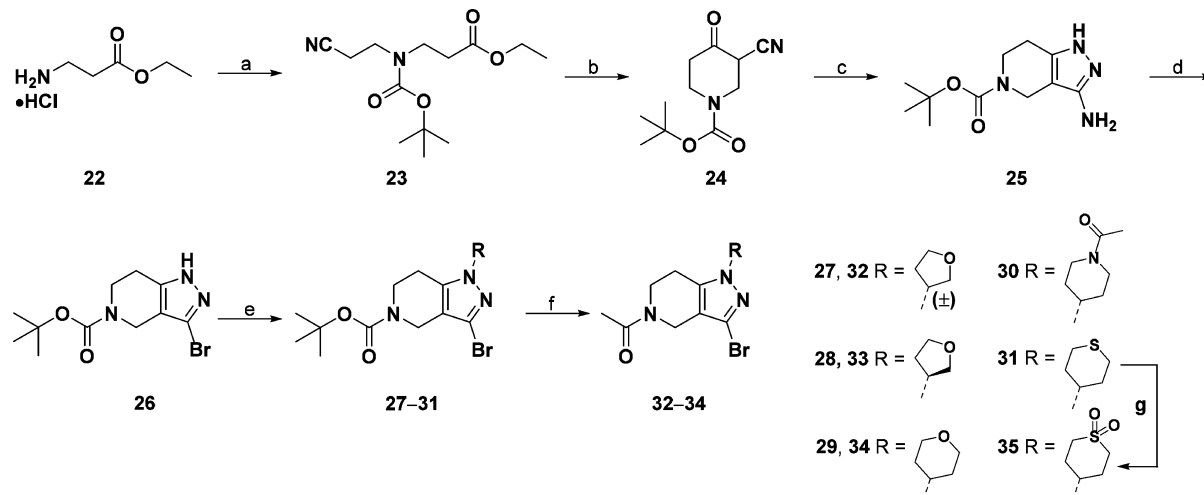


Figure 11. Compound **19** decreased the generation of iT_{reg}s in vitro without affecting cell viability. Human iT_{reg} cells were differentiated in vitro from naïve CD4+T cells derived from peripheral blood mononuclear cells (PBMCs) of a healthy donor in the presence of **19** or DMSO as control. On day 4, cells were harvested. (A) FOXP3 expression was assessed by q-RT-PCR and normalized with B2M. (B) Cell viability was assessed by flow cytometry using a fixable viability dye. (C) T_{reg} cells were also fixed, permeabilized, and intracellular FOXP3 protein assessed in CD4⁺CD25⁺ by flow cytometry. Graph shows % FOXP3+iT_{reg}s cells out of total CD4+T cells. Data are representative of three independent experiments.

mg/kg doses for **19**, resulting in comparable exposures and suppression of *MYC* transcript levels, corresponding to comparable efficacy for these two doses in the efficacy study.

At a dose of 30 mg/kg, we observed higher exposures of **19**, resulting in more durable suppression of *MYC* transcript levels, which corresponded to an increase in antitumor activity. These

Scheme 1. Synthesis of Intermediates 27–35^a

^aReagents and conditions: (a) (i) NaOH, acrylonitrile, MeOH, 70 °C, (ii) di-tert-butyl dicarbonate, 0 °C, 99%; (b) NaH, toluene, 100 °C, 100%; (c) hydrazine monohydrate, EtOH, 60 °C, 70%; (d) isopentyl nitrite, MeCN, CuBr₂, 60 °C, 34%; (e) R-OMs, Cs₂CO₃, DMF, 80 °C, 28–71%; (f) (i) TFA, DCM, rt, (ii) Ac₂O, TEA, DMF, rt, 77–87%; (g) oxone, THF, H₂O, rt, 98%.

data suggest that there is a dose-proportional PK–PD efficacy relationship where more durable suppression of MYC transcript results in better suppression of MOLM-16 tumor growth. Previously, we had evaluated **1** in this same xenograft model.¹² Compound **19**, possessing greater cell potency than **1**, exhibited approximately the same %TGI at 3 mg/kg as **1** does at 25 mg/kg (65% TGI). Taken together, these results demonstrate that **19** is highly active in vivo and capable of modulating CBP-dependent MYC transcription, which corresponds with antitumor activity in a MYC-dependent AML tumor model.

In addition to studying the effect of **19** in a hematologic antitumor xenograft model, we also explored the ability of this compound to impair T_{reg} differentiation and immunosuppressive function. CBP can interact with multiple transcription factors.²⁶ One of them is FOXP3, the master transcription factor defining T_{regs}. FOXP3 is essential for immune homeostasis, preventing autoimmunity, limiting chronic inflammation, and hampering effective immunity against tumors.^{27–30} Inhibition of the histone acetyltransferase domain of CBP has been shown to decrease the expression of FOXP3, leading to reduced tumor growth in mouse models of cancer.^{8,31} More recently, inhibition of the CBP bromodomain was also reported to impair FOXP3 expression and T_{reg} function, suggesting that bromodomain inhibition could impact optimal acetylation of chromatin associated transcription factors, including FOXP3 itself.¹⁰ To determine whether **19** would affect in vitro generation of inducible T_{regs} (iT_{regs}) and FOXP3 expression, human naïve CD4+T cells were differentiated toward T_{regs} using anti-CD3, anti-CD28, rIL-2, and rTGF β in the presence of increasing concentrations of **19** (0.001 to 2 μ M), using DMSO as a control. At day 4 postdifferentiation, cells were harvested, mRNA was extracted, and FOXP3 gene expression was assessed by quantitative reverse transcriptase polymerase chain reaction (q-RT-PCR). Figure 11A shows that **19** decreases FOXP3 transcripts in a dose-dependent manner ($IC_{50} = 17$ nM) consistent with the cellular potency in our MYC RNA assay. Moreover, the reduction in FOXP3 mRNA corresponded to a reduction in FOXP3 protein as determined in fixed and permeabilized CD4⁺CD25⁺ cells by fluorescence-activated cell sorting. Compound **19** did not affect cell viability (Figure 11B), and a dose-dependent decrease in FOXP3 staining

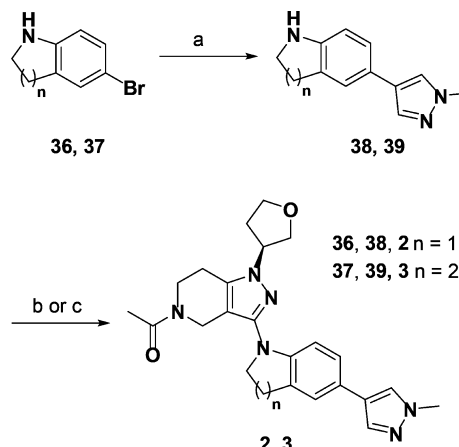
was observed (Figure 11C), corroborating the gene expression data. Taken together with our previous work,¹⁰ these data suggest that inhibition of the CBP bromodomain may provide a novel small molecule approach for cancer immunotherapy.

Chemistry. Intermediates **27–35** were prepared according to Scheme 1. Conjugate addition of ethyl 3-aminopropanoate (**22**) to acrylonitrile followed by Boc protection yielded **23**. Compound **23** was treated with sodium hydride and cyclized to give **24**. The pyrazolopiperidine core (**25**) was formed by treatment of **24** with hydrazine, and subsequent conversion of the amino function of **25** to the bromide under Sandmeyer conditions afforded **26**. Alkylation of the pyrazole **26** with the appropriate alkyl methanesulfonate yielded **27–31**. Deprotection of the Boc group with TFA followed by acylation with acetic anhydride afforded **32–34**. Intermediate sulfone **35** was formed by oxidation of thioether **31** with oxone.

The synthesis of **2** and **3** is outlined in Scheme 2. Suzuki coupling of 1-methyl-4-(4,4,5,5-tetramethyl-1,3,2-dioxaborolan-2-yl)-1*H*-pyrazole with commercially available **36** or **37** afforded **38** and **39**, respectively. Buchwald coupling of racemate **32** and **38** followed by chiral chromatography yielded **2**. (We have observed from evaluating analogues from the synthesis of enantiopure starting material that the (*R*)-isomer is always less potent than the (*S*)-isomer. Compound **2** was assumed to be the (*S*)-isomer as this was more potent than the (*R*)-isomer.) Buchwald coupling of optically pure **33** with **39** afforded **3**.

Buchwald coupling of commercially available **40** or **41** with intermediate **33** yielded **42** and **43**, respectively (Scheme 3). Bromination of **42** and **43** with *N*-bromosuccinimide (NBS) gave bromides **44** and **45**, respectively. Subsequent Suzuki coupling with 1-methyl-4-(4,4,5,5-tetramethyl-1,3,2-dioxaborolan-2-yl)pyrazole provided analogues **4** and **7**, respectively.

Scheme 4 shows the synthesis of compounds **5**, **6**, **8**, and **9**. Appropriately substituted THQs (**46–48**) were treated with NBS, yielding the brominated intermediates **49–51**. Suzuki coupling of **49–51** with 1-methyl-4-(4,4,5,5-tetramethyl-1,3,2-dioxaborolan-2-yl)-1*H*-pyrazole provided **52–54**. Buchwald coupling of intermediate **33** with **52** or **54** provided compounds **6** and **9**, respectively. Buchwald coupling of racemic intermediate **32** with **53** followed by chiral chromatography yielded **8**.

Scheme 2. Synthesis of Compounds 2 and 3^a

^aReagents and conditions: (a) 1-methyl-4-(4,4,5,5-tetramethyl-1,3,2-dioxaborolan-2-yl)-1H-pyrazole, Pd(dppf)Cl₂, Na₂CO₃ or K₂CO₃, dioxane, H₂O, 120 °C, 47–86%; (b) 32, RuPhos Pd G1, RuPhos, t-BuONa, dioxane, 120 °C, supercritical fluid chromatography (SFC) chiral resolution, 16%; (c) 33, RuPhos Pd G1, RuPhos, t-BuONa, dioxane, 120 °C, 34%

Chloride 6 was converted directly to methyl analogue 5 via palladium coupling with potassium methyltrifluoroborate.

Buchwald coupling of intermediate 34 with THQ 53 afforded 10 (Scheme 5).

The syntheses of 11–13 and 15 are shown in Scheme 6. Treatment of intermediate 26 with SEM-Cl followed by Buchwald coupling with 53 provided 56. Removal of the SEM and Boc protecting groups yielded 58. Acetylation of the piperidine with acetic anhydride afforded the key intermediate 59. Alkylation of 59 with the corresponding bromide or mesylate yielded 11, 15, and 60. Compound 60 was further converted to 13 by first removing the Boc group followed by reductive amination with formaldehyde.

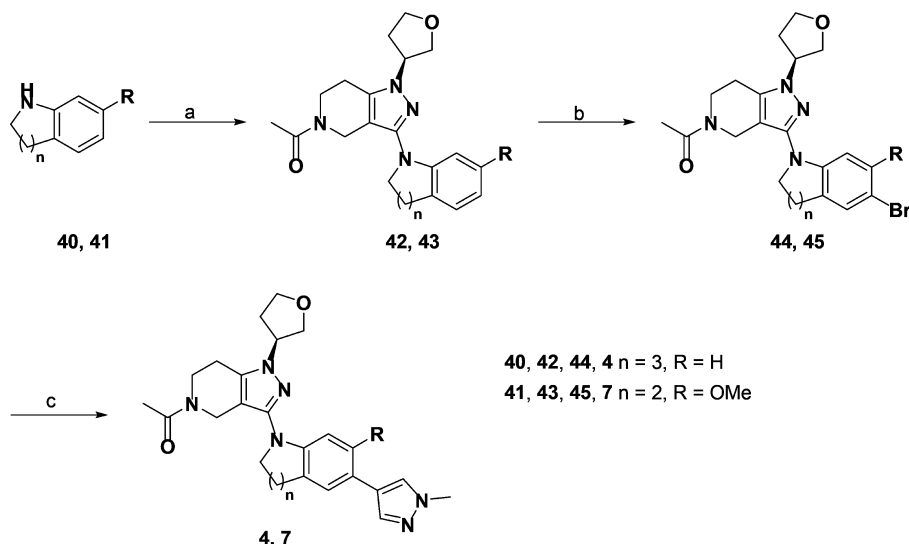
Outlined in Scheme 7 is the synthesis of 14 and 16. Buchwald coupling of 30 or 35 with THQ 53 provided 61 and 62,

respectively. Deprotection of the Boc group with TFA followed by acetylation with acetic anhydride afforded candidate compounds 14 and 16.

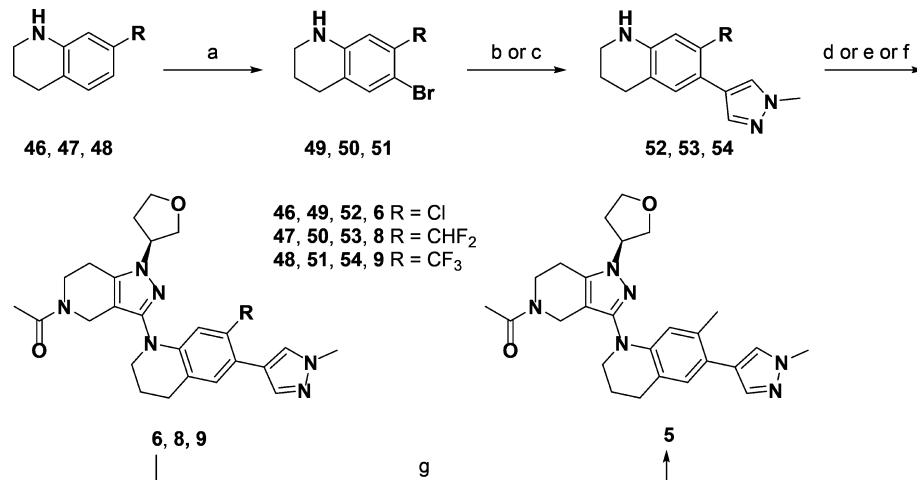
Buchwald coupling of THQ 53 with 29 to form 65, followed by deprotection of the Boc group with TFA, yielded key intermediate 66 from which urea analogues 18–21 could be synthesized (Scheme 8). Compound 66 was treated with (trimethylsilyl)isocyanate to afford the unsubstituted urea 18. Monomethyl urea 19 was formed from treatment of 66 with N-methyl-1*H*-imidazole-1-carboxamide. Intermediate 66 was first treated with 4-nitrophenyl chloroformate then with ethylamine to yield 20. Dimethyl urea 21 was synthesized by treatment of 66 with dimethylcarbamoyl chloride.

CONCLUSION

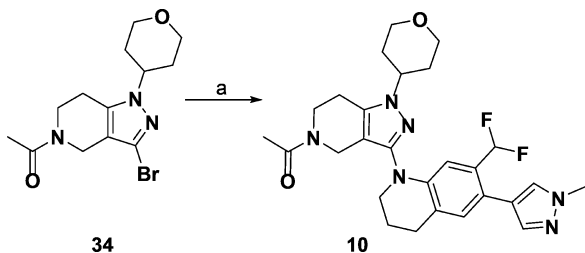
We have identified a highly potent and selective in vivo probe (19) of the CBP bromodomain that is suitable to interrogate the biology of CBP without the complication of BET inhibition. Our studies began with recently disclosed 1 (TR-FRET IC₅₀ = 20 nM, BRET IC₅₀ = 410 nM, BRD4(1) IC₅₀ = 13,000 nM) that was moderately potent for the bromodomain of CBP and 650-fold selective over BRD4(1). Constraining the aniline of 1 into tetrahydroquinoline 3 maintained potency and increased selectivity by 2-fold over 1. Structure–activity relationship studies coupled with structure-based design targeting the LPF shelf, BC loop, and KAc regions allowed us to identify 10 (TR-FRET IC₅₀ = 1.1 nM, BRET IC₅₀ = 12 nM, BRD4(1) IC₅₀ = 4200 nM). Further profiling of this compound revealed that it penetrated into the CNS, resulting in adverse CNS effects. Subsequent optimization focused on increasing tPSA with the addition of a hydrogen bond donor. This was accomplished with conversion of the Asn-binding acetamide of 10 to a methyl urea, enabling identification of non-CNS penetrant 19 (TR-FRET IC₅₀ = 0.94 nM, BRET IC₅₀ = 6.2 nM, BRD4(1) IC₅₀ = 5100 nM) that demonstrated an appropriate balance of cell potency, selectivity (5425-fold over BRD4(1)), and in vivo PK. The exquisite potency and selectivity of 19 enables the clear delineation of pharmacological effects from the inhibition of

Scheme 3. Synthesis of Compounds 4 and 7^a

^aReagents and conditions: (a) 33, RuPhos Pd G1, RuPhos, t-BuONa, dioxane, 120 °C, 26–39%; (b) NBS, DCM, 0 °C to rt 90–97%; (c) 1-methyl-4-(4,4,5,5-tetramethyl-1,3,2-dioxaborolan-2-yl)-1H-pyrazole, Pd(dppf)Cl₂, K₂CO₃, dioxane, H₂O, 110 °C, 23–24%.

Scheme 4. Synthesis of Compounds 5, 6, 8, and 9^a

^aReagents and conditions: (a) NBS, DCM, 0 °C to rt, 36–60%; (b) 1-methyl-4-(4,4,5,5-tetramethyl-1,3,2-dioxaborolan-2-yl)-1H-pyrazole, Pd(dppf)Cl₂, K₂CO₃ or Na₂CO₃, dioxane, H₂O, 110 °C, 86–95%; (c) 1-methyl-4-(4,4,5,5-tetramethyl-1,3,2-dioxaborolan-2-yl)-1H-pyrazole, XPhos Pd G2, XPhos, Na₂CO₃, THF, H₂O, 80 °C, 70%; (d) 33, Pd₂(dba)₃, XantPhos, t-BuONa, dioxane, toluene, 90 °C, 50%; (e) 32, RuPhos Pd G1, RuPhos, t-BuONa, dioxane, 130 °C, SFC chiral resolution, 16%; (f) 33, Pd-PEPPSI-IPent, t-BuONa, dioxane, 150 °C, 21%; (g) 6, Ad₂PBu, MeBF₃K, Pd(OAc)₂, Cs₂CO₃, toluene, H₂O, 100 °C, 15%.

Scheme 5. Synthesis of Compound 10^a

CBP over the BET bromodomains. In vivo, **19** modulates MYC expression that corresponds with antitumor activity in an AML tumor model. Additional in vitro studies with **19** showed that this compound impaired FOXP3 expression and T_{reg} function, further suggesting CBP bromodomain inhibition as a novel small molecule approach for cancer immunotherapy.

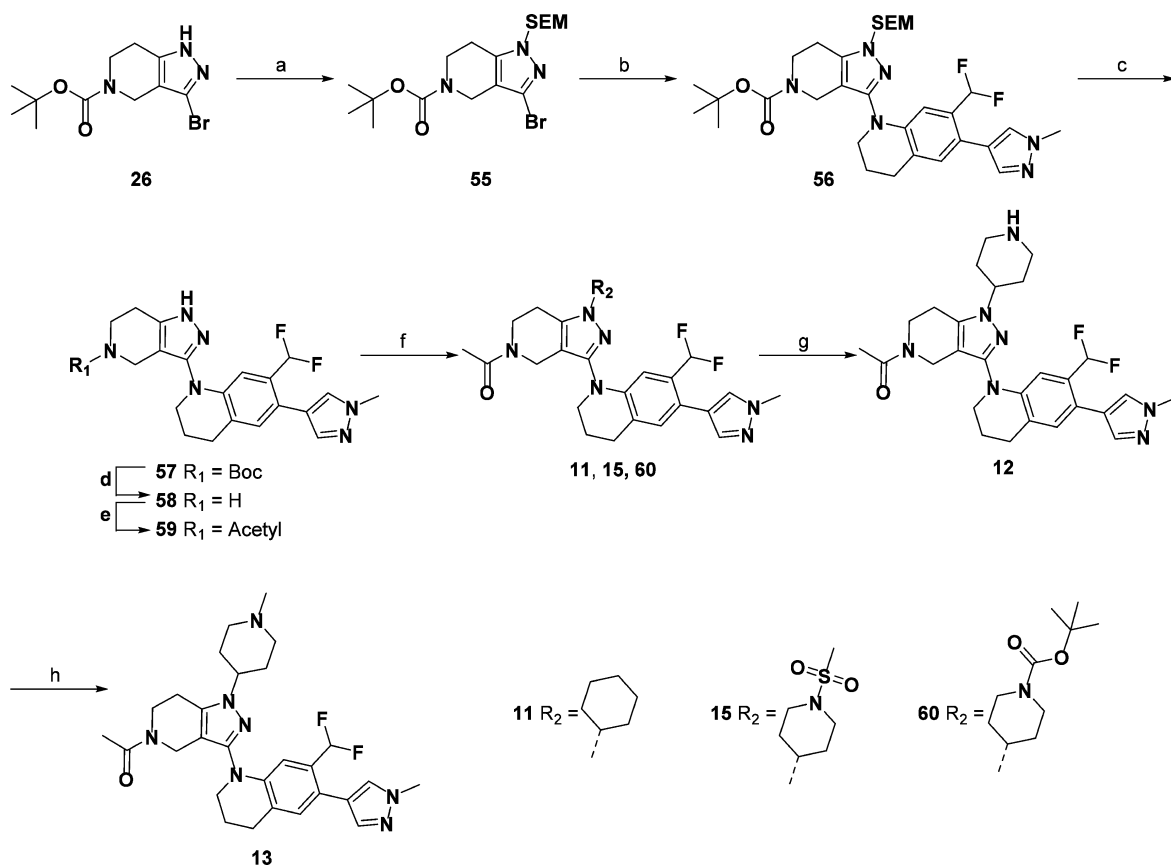
EXPERIMENTAL PROCEDURES

General Methods. All solvents and reagents were used as obtained. NMR analysis performed in a deuterated solvent with a Varian Avance 300 MHz or Bruker Avance 400 or 500 MHz NMR spectrometers, referenced to trimethylsilane (TMS). Chemical shifts are expressed as δ units using TMS as the external standard (in NMR description, s = singlet, d = doublet, t = triplet, q = quartet, m = multiplet, and br = broad peak). All coupling constants (J) are reported in hertz. Compounds with the acetamide moiety (e.g., compound **10**) exhibited rotamers in the NMR, and thus in many cases coupling constants were not reported and generally characterized as multiplets. In addition, the ¹³C of compound **10** was run at elevated temperature in order to coalesce the multiple rotamer peaks into a single peak. Mass spectra were measured with a Finnigan SSQ710C spectrometer using an ESI source coupled to a Waters 600MS high performance liquid chromatography (HPLC) system operating in reverse-phase mode with an X-bridge phenyl column of dimensions 150 mm by 2.6 mm, with 5 μ m sized particles. Preparatory-scale silica gel chromatography was performed using medium-pressure liquid chromatography (MPLC) on a CombiFlash Companion (Teledyne ISCO) with RediSep normal phase silica gel

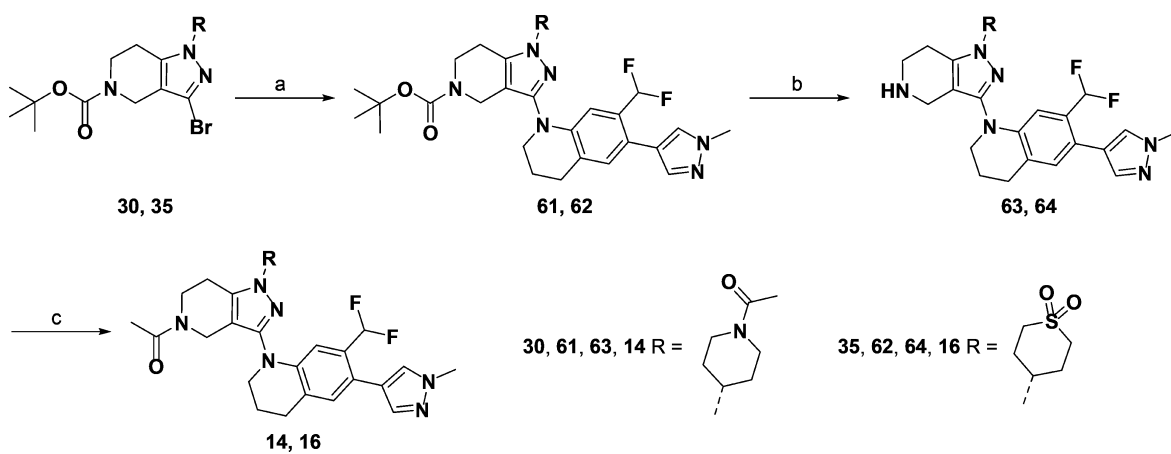
(35–60 μ m) columns and UV detection at 254 nm. Reverse-phase (HPLC) was used to purify compounds as needed by elution from a Phenomenex Gemini-NX C18 column (20.2 mm × 50 mm, 5 μ m) as stationary phase using mobile phase indicated and operating at a 35 mL/min flow rate on a Waters 3100 mass-directed prep instrument. Chemical purities were >95% for all final compounds as assessed by LC/MS analysis. The following analytical method was used to determine chemical purity of final compounds: HPLC-Agilent 1200, water with 0.05% TFA, acetonitrile with 0.05% TFA (buffer B), Agilent SB-C18, 1.8 μ m, 2.1 mm × 30 mm, 25 °C, 3–95% buffer B in 8.5 min, 95% in 2.5 min, 400 μ L/min, 220 and 254 nm, equipped with Agilent quadrupole 6140, ESI positive, 90–1300 amu.

tert-Butyl 3-Bromo-1-(tetrahydrofuran-3-yl)-6,7-dihydro-1H-pyrazolo[4,3-c]pyridine-5(4H)-carboxylate (27). Step 1: Ethyl 3-((tert-butoxycarbonyl)(2-cyanoethyl)amino)propanoate (23). To a solution of ethyl 3-aminopropanoate hydrochloride (22, 367 g, 2.39 mol) in MeOH (1.2 L) at room temperature was added NaOH (95.6 g, 2.39 mol) portionwise. The mixture was heated to 70 °C, acrylonitrile (158 g, 2.98 mol) was added dropwise, and the reaction mixture was stirred for 6 h. The solution was cooled to 0 °C before di-*tert*-butyl dicarbonate (521 g, 2.39 mol) was added. The reaction was stirred at room temperature for 6 h, filtered, and washed with MeOH (200 mL). The filtrate was concentrated in vacuo to give a yellow oily residue that was redissolved in EtOAc and water (500 mL). The aqueous layer was extracted with EtOAc (800 mL). The combined organic layers were dried over anhydrous Na₂SO₄, filtered, and concentrated in vacuo to give the title compound (23, 638 g, 99%) as a light-yellow oil that required no further purification. ¹H NMR (400 MHz, CDCl₃) δ 4.17 (q, J = 7.2 Hz, 2H), 3.68–3.62 (m, 4H), 2.57–2.53 (m, 4H), 1.49 (s, 9H), 1.29 (t, J = 7.2 Hz, 3H).

Step 2: *tert*-Butyl 3-Cyano-4-oxopiperidine-1-carboxylate (24). To toluene (2.7 L) at 25 °C was added NaH (80 g, 2.0 mol) portionwise, and the suspension was heated to 80 °C. Ethyl 3-((tert-butoxycarbonyl)-(2-cyanoethyl)amino)propanoate (23, 270 g, 1.00 mol) in anhydrous toluene (270 mL) was added dropwise. The mixture was heated to 100 °C and stirred for 5 h. The mixture was cooled to room temperature, quenched with satd aq ammonium chloride (800 mL), and washed with hexanes (800 mL). The aqueous phase was acidified with HCl (2N) to pH 6, and the mixture was extracted with EtOAc (1 L × 2). The combined organic layers were dried over anhydrous Na₂SO₄, filtered, and concentrated in vacuo to give *tert*-butyl 3-cyano-4-oxopiperidine-1-carboxylate (24, 310 g, 100%) as yellow oil that required no further

Scheme 6. Synthesis of Compounds 11–13 and 15^a

^aReagents and conditions: (a) NaH, SEM-Cl, THF, 0 °C to rt, 83%; (b) 53, RuPhos Pd G2, RuPhos, t-BuONa, dioxane, 120 °C, 20%; (c) TBAF, THF, 60 °C, 66%; (d) TFA, DCM, rt, 100%; (e) Ac₂O, TEA, DMF, rt, 14%; (f) R₂-Br or R₂-OMs, Cs₂CO₃, DMF, 80 °C, 5–17%; (g) 60, TFA, DCM, 0 °C to rt, 49%; (h) aq CH₂O, CH₃CO₂H, NaBH(OAc)₃, DCE, rt, 23%.

Scheme 7. Synthesis of Compounds 14 and 16^a

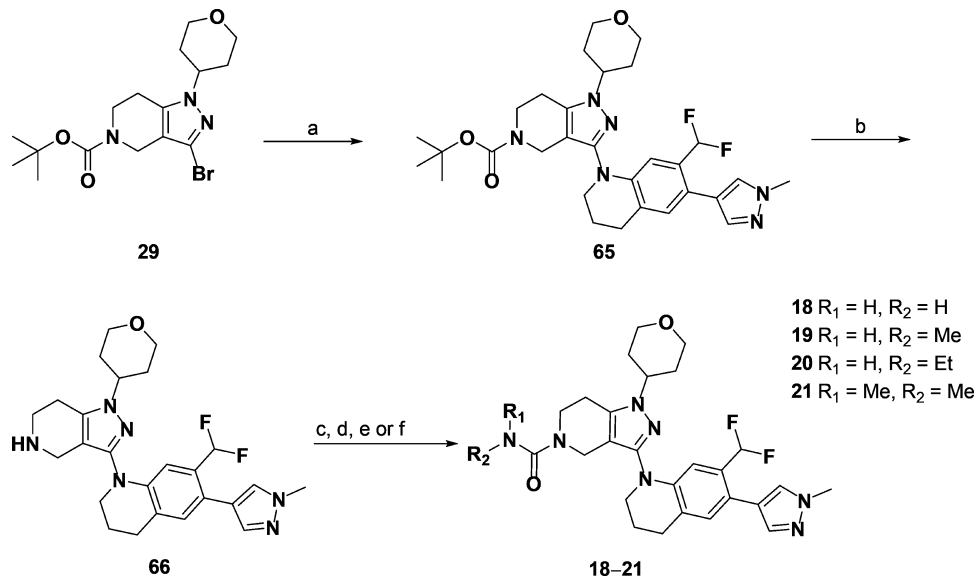
^aReagents and conditions: (a) 53, Pd-PEPPSI-IPent, t-BuONa, dioxane, 120 °C, 42–46%; (b) TFA, DCM, rt, 100%; (c) Ac₂O, TEA, DCM, 0 °C to rt, 40–52%.

purification. ¹H NMR (400 MHz, CDCl₃) δ 4.17–4.14 (m, 1H), 3.59–3.56 (m, 2H), 3.43–3.41 (m, 2H), 2.70–2.66 (m, 2H), 1.51 (s, 9H).

Step 3: *tert*-Butyl 3-Amino-6,7-dihydro-1*H*-pyrazolo[4,3-*c*]pyridine-5(4*H*)-carboxylate (**25**). A mixture of *tert*-butyl 3-cyano-4-oxopiperidine-1-carboxylate (**24**, 310 g, 1.38 mol) and hydrazine monohydrate (140 mL, 2.08 mol) in EtOH (1.5 L) was heated to 60 °C for 2 h. The mixture was concentrated in vacuo to give the crude product that was dissolved in EtOAc (1 L) and washed with water (1 L × 2). The organic layer was dried over anhydrous Na₂SO₄, filtered, and

concentrated in vacuo to afford *tert*-butyl 3-amino-6,7-dihydro-1*H*-pyrazolo[4,3-*c*]pyridine-5(4*H*)-carboxylate (**25**, 230 g, 70%) as a colorless solid. ¹H NMR (400 MHz, CD₃OD) δ 4.28 (s, 2H), 3.66–3.63 (m, 2H), 2.62–2.59 (m, 2H), 1.49 (s, 9H).

Step 4: *tert*-Butyl 3-Bromo-6,7-dihydro-1*H*-pyrazolo[4,3-*c*]pyridine-5(4*H*)-carboxylate (**26**). To a stirred mixture of *tert*-butyl 3-amino-6,7-dihydro-1*H*-pyrazolo[4,3-*c*]pyridine-5(4*H*)-carboxylate (**25**, 120 g, 504 mmol), CuBr₂ (112.5 g, 503.6 mmol), and MeCN (1.2 L) at 0 °C was added isopropyl nitrite (76.7 g, 655 mmol), and the reaction

Scheme 8. Synthesis of Compounds 18–21^a

^a Reagents and conditions: (a) 53, RuPhos Pd G1, RuPhos, *t*-BuONa, dioxane, 120 °C, 73%; (b) TFA, DCM, rt; (c) TMSNCO, DCM, rt, 20%; (d) *N*-methyl-1*H*-imidazole-1-carboxamide, DCM, rt, 22%; (e) (i) 4-nitrophenyl chloroformate, pyridine, DMF, rt, (ii) EtNH₂, THF, rt, 14%; (f) dimethylcarbamyl chloride, TEA, DMF, rt, 22%.

mixture stirred for 20 min. The temperature was raised to 60 °C, and the reaction mixture was stirred for an additional 5 h. After cooling the reaction to room temperature, the reaction mixture was quenched with water (1 L) and the mixture was extracted with EtOAc (1 L × 2). The combined organic layers were dried over anhydrous Na₂SO₄, filtered, and concentrated in vacuo. The crude residue was purified by silica gel chromatography (petroleum ether/EtOAc = 4:1) to afford *tert*-butyl 3-bromo-6,7-dihydro-1*H*-pyrazolo[4,3-*c*]pyridine-5(4*H*)-carboxylate (**26**, 52 g, 34%) as light-yellow solid. LCMS *m/z* (M + H) 302.

Step 5: *tert*-Butyl 3-Bromo-1-(tetrahydrofuran-3-yl)-6,7-dihydro-1*H*-pyrazolo[4,3-*c*]pyridine-5(4*H*)-carboxylate (27). To a solution of *tert*-butyl 3-bromo-6,7-dihydro-1*H*-pyrazolo[4,3-*c*]pyridine-5(4*H*)-carboxylate (**26**, 20.0 g, 66.0 mmol) in DMF (100 mL) was added Cs₂CO₃ (40.0 g, 123 mmol) and tetrahydrofuran-3-yl methanesulfonate (16.0 g, 98.0 mmol). The mixture was heated to 80 °C for 12 h. The solution was concentrated in vacuo, and the crude residue was purified by silica gel chromatography (eluent from petroleum ether/EtOAc = 10:1 to 3:1) to give the title compound (**27**, 17 g, 69%) as a yellow oil. ¹H NMR (400 MHz, CDCl₃) δ 4.78–4.69 (m, 1H), 4.26 (s, 2H), 4.18–3.86 (m, 4H), 3.72 (s, 2H), 2.72–2.62 (m, 2H), 2.44–2.22 (m, 2H), 1.48 (s, 9H).

(S)-*tert*-Butyl 3-Bromo-1-(tetrahydrofuran-3-yl)-6,7-dihydro-1*H*-pyrazolo[4,3-*c*]pyridine-5(4*H*)-carboxylate (28). In a similar manner to **27**, compound **28** was prepared from (R)-tetrahydrofuran-3-yl methanesulfonate to provide the title compound (71%) as a yellow oil. ¹H NMR (400 MHz, DMSO-*d*₆) δ 4.97–4.78 (m, 1H), 4.13 (s, 2H), 3.98–3.86 (m, 2H), 3.81–3.67 (m, 2H), 3.56 (*t*, *J* = 5.6 Hz, 2H), 2.68 (*t*, *J* = 5.6 Hz, 2H), 2.33–2.08 (m, 2H), 1.38 (s, 9H).

***tert*-Butyl 3-Bromo-1-(tetrahydro-2*H*-pyran-4-yl)-6,7-dihydro-1*H*-pyrazolo[4,3-*c*]pyridine-5(4*H*)-carboxylate (29).** In a similar manner to **27**, compound **29** was prepared from tetrahydro-2*H*-pyran-4-yl methanesulfonate to provide the title compound (47%) as a colorless oil. ¹H NMR (400 MHz, DMSO-*d*₆) δ 4.35–4.25 (m, 1H), 4.17 (s, 2H), 3.95–3.93 (m, 2H), 3.62–3.57 (m, 2H), 3.42 (*t*, *J* = 11.2 Hz, 2H), 2.74–2.73 (m, 2H), 1.98–1.89 (m, 2H), 1.80–1.77 (m, 2H), 1.41 (s, 9H).

***tert*-Butyl 1-(1-Acetylpiridin-4-yl)-3-bromo-6,7-dihydro-1*H*-pyrazolo[4,3-*c*]pyridine-5(4*H*)-carboxylate (30).** In a similar manner to **27**, compound **30** was prepared from 1-acetylpiridin-4-yl methanesulfonate to provide the title compound (28%) as a yellow solid. ¹H NMR (400 MHz, DMSO-*d*₆) δ 4.50–4.41 (m, 1H), 4.38–4.29 (m, 1H), 4.16 (s, 2H), 3.94–3.85 (m, 1H), 3.64–3.57 (m, 2H), 3.21–

3.09 (m, 1H), 2.75–2.58 (m, 3H), 2.03 (s, 3H), 1.91–1.80 (m, 3H), 1.73–1.61 (m, 1H), 1.41 (s, 9H).

***tert*-Butyl 3-Bromo-1-(1,1-dioxidotetrahydro-2*H*-thiopyran-4-yl)-6,7-dihydro-1*H*-pyrazolo[4,3-*c*]pyridine-5(4*H*)-carboxylate (35).** **Step 1:** *tert*-Butyl 3-Bromo-1-(tetrahydro-2*H*-thiopyran-4-yl)-6,7-dihydro-1*H*-pyrazolo[4,3-*c*]pyridine-5(4*H*)-carboxylate (**31**). To a solution of *tert*-butyl 3-bromo-6,7-dihydro-1*H*-pyrazolo[4,3-*c*]pyridine-5(4*H*)-carboxylate (**26**, 10.0 g, 33.1 mmol) in DMF (50 mL) was added Cs₂CO₃ (27.0 g, 82.7 mmol) and tetrahydro-2*H*-thiopyran-4-yl methanesulfonate (8.4 g, 43.0 mmol). The mixture was heated to 80 °C for 16 h under a nitrogen atmosphere. After cooling the reaction to room temperature, the mixture was filtered. The mixture was diluted with EtOAc (100 mL) and washed with brine (100 mL × 2). The organic layer was dried over anhydrous Na₂SO₄, filtered, and concentrated in vacuo. The crude residue was purified by silica gel chromatography (eluent from petroleum ether/*tert*-butyl methyl ether/THF = from 10:1:1 to 3:1:1) to give the title compound (**31**, 5.9 g, 44%) as a white solid. ¹H NMR (400 MHz, DMSO-*d*₆) δ 4.17 (s, 2H), 4.09–4.04 (m, 1H), 3.62–3.59 (m, 2H), 2.83–2.77 (m, 2H), 2.71–2.68 (m, 4H), 2.13–2.10 (m, 2H), 2.03–1.93 (m, 2H), 1.44 (s, 9H).

Step 2: *tert*-Butyl 3-Bromo-1-(1,1-dioxidotetrahydro-2*H*-thiopyran-4-yl)-6,7-dihydro-1*H*-pyrazolo[4,3-*c*]pyridine-5(4*H*)-carboxylate (35). To a solution of *tert*-butyl 3-bromo-1-(tetrahydro-2*H*-thiopyran-4-yl)-6,7-dihydro-1*H*-pyrazolo[4,3-*c*]pyridine-5(4*H*)-carboxylate (**31**, 2.0 g, 5.0 mmol) in THF (10 mL) and water (2 mL) at 0 °C was added oxone (3.1 g, 5 mmol) portionwise. The mixture was stirred at room temperature for 2 h. The reaction was quenched by satd aq Na₂SO₃ and extracted with DCM (20 mL × 3). The combined organic layers were dried over anhydrous Na₂SO₄, filtered, and concentrated in vacuo to give the title compound (**35**, 2.1 g, 98%) as a white solid that required no further purification. LCMS *m/z* (M + H) 436.

1-(3-Bromo-1-(tetrahydrofuran-3-yl)-6,7-dihydro-1*H*-pyrazolo[4,3-*c*]pyridin-5(4*H*)-yl)ethanone (32). To a solution of *tert*-butyl 3-bromo-1-(tetrahydrofuran-3-yl)-6,7-dihydro-1*H*-pyrazolo[4,3-*c*]pyridine-5(4*H*)-carboxylate (**27**, 17.0 g, 45.0 mmol) in DCM (60 mL) was added TFA (30 mL) dropwise. The reaction solution was stirred at room temperature for 2 h. The solvent was removed by evaporation, and the crude product was redissolved in DMF (50 mL). The mixture was cooled to 0 °C before TEA (41.0 g, 40.5 mmol) and acetic anhydride (7.00 g, 68.0 mmol) were added dropwise. The ice bath was removed, and the reaction was stirred at room temperature for additional 2 h. Water (50 mL) was added, and the solution was extracted

with EtOAc (150 mL \times 3). The combined organic layers were dried over anhydrous Na₂SO₄, filtered, and concentrated in vacuo. The crude residue was purified by silica gel chromatography (DCM/MeOH = 30:1) to give the title compound (32, 12.0 g, 82%) as a white solid. ¹H NMR (400 MHz, DMSO-*d*₆) δ 4.96–4.92 (m, 1H), 4.28 (s, 2H), 3.99–3.95 (m, 2H), 3.80–3.68 (m, 4H), 2.82–2.70 (m, 2H), 2.29–2.19 (m, 2H), 2.10–2.08 (m, 3H).

(*S*)-1-(3-Bromo-1-(tetrahydrofuran-3-yl)-6,7-dihydro-1*H*-pyrazolo[4,3-*c*]pyridin-5(4*H*)-yl)ethanone (33). In a similar manner to 32, compound 33 was prepared from (*S*-*tert*-butyl 3-bromo-1-(tetrahydrofuran-3-yl)-6,7-dihydro-1*H*-pyrazolo[4,3-*c*]pyridine-5(4*H*)-carboxylate (28) to provide the title compound (87%) as a white solid. ¹H NMR (400 MHz, CDCl₃) δ 4.78–4.67 (m, 1H), 4.45–4.29 (m, 2H), 4.15–4.06 (m, 2H), 3.96–3.92 (m, 2H), 3.88–3.70 (m, 2H), 2.71–2.67 (m, 2H), 2.38–2.34 (m, 2H), 2.16 (s, 3H).

1-(3-Bromo-1-(tetrahydro-2*H*-pyran-4-yl)-6,7-dihydro-1*H*-pyrazolo[4,3-*c*]pyridin-5(4*H*)-yl)ethanone (34). In a similar manner to 32, compound 34 was prepared from *tert*-butyl 3-bromo-1-(tetrahydro-2*H*-pyran-4-yl)-6,7-dihydro-1*H*-pyrazolo[4,3-*c*]pyridine-5(4*H*)-carboxylate (29) to provide the title compound (77%) as a light-yellow solid. ¹H NMR (400 MHz, DMSO-*d*₆) δ 4.33–4.29 (m, 1H), 4.28 (s 2H), 3.95–3.92 (m, 2H), 3.70–3.67 (m, 2H), 3.43–3.36 (m, 2H), 2.84–2.69 (m, 2H), 2.09–2.08 (m, 3H), 1.96–1.91 (m, 2H), 1.80–1.76 (m, 2H).

1-[3-[5-(1-Methylpyrazol-4-yl)indolin-1-yl]-1-[(3*S*)-tetrahydrofuran-3-yl]-6,7-dihydro-4*H*-pyrazolo[4,3-*c*]pyridin-5-yl]ethanone (2). Step 1: 5-(1-Methyl-1*H*-pyrazol-4-yl)indoline (38). To a solution of 5-bromoindoline (36, 500 mg, 2.52 mmol), 1-methyl-4-(4,4,5,5-tetramethyl-1,3,2-dioxaborolan-2-yl)-1*H*-pyrazole (630 mg, 3.03 mmol), and Na₂CO₃ (535 mg, 5.05 mmol) in dioxane (20 mL) and H₂O (5 mL) was added [1,1'-bis(diphenylphosphino)ferrocene]-dichloropalladium(II) (184 mg, 0.250 mmol). The mixture was heated to 120 °C for 12 h under a nitrogen atmosphere. After cooling to room temperature, the mixture was filtered and the filtrate was concentrated in vacuo. The crude residue was purified by silica gel chromatography (petroleum ether/EtOAc = 1:1) to give the presumed title compound (38, 430 mg, 86%) as a light yellow solid.

Step 2: 1-[3-[5-(1-Methylpyrazol-4-yl)indolin-1-yl]-1-tetrahydrofuran-3-yl]-6,7-dihydro-4*H*-pyrazolo[4,3-*c*]pyridin-5-yl]ethanone. To a solution of 1-(3-bromo-1-(tetrahydrofuran-3-yl)-6,7-dihydro-1*H*-pyrazolo[4,3-*c*]pyridin-5(4*H*)-yl)ethanone (32, 500 mg, 1.59 mmol), 5-(1-methyl-1*H*-pyrazol-4-yl)indoline (38, 371 mg, 1.59 mmol), and *t*-BuONa (458 mg, 4.77 mmol) in 1,4-dioxane (10 mL) was added chloro(2-dicyclohexylphosphino-2',6'-di-*I*-propoxy-1,1'-biphenyl)[2-(2-aminoethylphenyl)]palladium(II), methyl-*tert*-butylether adduct (130 mg, 0.160 mmol) and 2-dicyclohexylphosphino-2',6'-di-*I*-propoxy-1,1'-biphenyl (74 mg, 0.16 mmol). The mixture was heated to 120 °C for 12 h under a nitrogen atmosphere. After cooling to room temperature, the mixture was filtered and the filtrate was concentrated in vacuo. The crude residue was purified by reverse phase chromatography (acetonitrile 32–62%/0.1% NH₄OH in water) to give the title compound (112 mg, 16%) as a white solid. ¹H NMR (400 MHz, CDCl₃) δ 7.69 (s, 1H), 7.51 (s, 1H), 7.41–7.13 (m, 3H), 4.74–4.71 (m, 1H), 4.68–4.48 (m, 2H), 4.12–4.06 (m, 2H), 4.04–4.01 (m, 4H), 3.99 (s, 3H), 3.93–3.75 (m, 2H), 3.21–3.17 (m, 2H), 2.73–2.70 (m, 2H), 2.45–2.32 (m, 2H), 2.20–2.15 (m, 3). LCMS *m/z* (M + H) 433.

Step 3: 1-[3-[5-(1-Methylpyrazol-4-yl)indolin-1-yl]-1-[(3*S*)-tetrahydrofuran-3-yl]-6,7-dihydro-4*H*-pyrazolo[4,3-*c*]pyridin-5-yl]ethanone (2). Racemic 1-[3-[5-(1-methylpyrazol-4-yl)indolin-1-yl]-1-tetrahydrofuran-3-yl]-6,7-dihydro-4*H*-pyrazolo[4,3-*c*]pyridin-5-yl]ethanone (100 mg) was separated by using chiral SFC (Chiralcel OJ 250 mm \times 30 mm I.D., 10 μm; Supercritical CO₂/MeOH (0.1% NH₃ H₂O) = 50/50 at 70 mL/min) to give 1-[3-[5-(1-methylpyrazol-4-yl)indolin-1-yl]-1-[(3*R*)-tetrahydrofuran-3-yl]-6,7-dihydro-4*H*-pyrazolo[4,3-*c*]pyridin-5-yl]ethanone (26 mg, first peak) and 1-[3-[5-(1-methylpyrazol-4-yl)indolin-1-yl]-1-[(3*S*)-tetrahydrofuran-3-yl]-6,7-dihydro-4*H*-pyrazolo[4,3-*c*]pyridin-5-yl]ethanone (29 mg, second peak). Absolute configuration was arbitrarily assigned to each enantiomer. Isomer A: ¹H NMR (400 MHz, DMSO-*d*₆) δ 7.94 (s, 1H), 7.72 (s, 1H), 7.42–7.32 (m, 2H), 7.26–7.23 (m, 1H), 4.89–4.83 (m, 1H), 4.55–4.53 (m, 2H),

4.05–3.97 (m, 4H), 3.86–3.70 (m, 7H), 3.14–3.10 (m, 2H), 2.80–2.67 (m, 2H), 2.26–2.23 (m, 2H), 2.10–2.28 (m, 3H). LCMS *m/z* (M + H) 433. Isomer B (2): ¹H NMR (400 MHz, DMSO-*d*₆) δ 7.94 (s, 1H), 7.72 (s, 1H), 7.42–7.32 (m, 2H), 7.26–7.23 (m, 1H), 4.88–4.86 (m, 1H), 4.55–4.53 (m, 2H), 4.03–3.96 (m, 4H), 3.86–3.70 (m, 7H), 3.14–3.10 (m, 2H), 2.80–2.67 (m, 2H), 2.26–2.24 (m, 2H), 2.10–2.28 (m, 3H). LCMS *m/z* (M + H) 433.

1-[3-[6-(1-Methylpyrazol-4-yl)-3,4-dihydro-2*H*-quinolin-1-yl]-1-[(3*S*)-tetrahydrofuran-3-yl]-6,7-dihydro-4*H*-pyrazolo[4,3-*c*]pyridin-5-yl]ethanone (3). Step 1: 6-(1-Methyl-1*H*-pyrazol-4-yl)-1,2,3,4-tetrahydroquinoline (39). To a solution of 6-bromo-1,2,3,4-tetrahydroquinoline (37, 17.0 g, 80.2 mmol), 1-methyl-4-(4,4,5,5-tetramethyl-1,3,2-dioxaborolan-2-yl)-1*H*-pyrazole (25.0 g, 120.2 mmol), and K₂CO₃ (33.2 g, 240 mmol) in dioxane/H₂O (5:1, 150 mL) was added [1,1'-bis(diphenylphosphino)ferrocene]-dichloropalladium(II) (5.80 g, 8.02 mmol). The mixture was heated to 120 °C for 16 h under a nitrogen atmosphere. After cooling the reaction to room temperature, the mixture was filtered and the filtrate was concentrated in vacuo. The crude residue was purified by silica gel chromatography (petroleum ether/EtOAc = 1:1) to give the title compound (39, 8.0 g, 47%) as a yellow solid. ¹H NMR (400 MHz, CD₃OD) δ 7.71 (s, 1H), 7.62 (s, 1H), 7.07 (d, *J* = 6.0 Hz, 2H), 6.50 (d, *J* = 8.4 Hz, 1H), 3.87 (s, 3H), 3.23 (t, *J* = 5.2 Hz, 2H), 2.75 (t, *J* = 6.4 Hz, 2H), 1.94–1.88 (m, 2H).

Step 2: 1-[3-[6-(1-Methylpyrazol-4-yl)-3,4-dihydro-2*H*-quinolin-1-yl]-1-[(3*S*)-tetrahydrofuran-3-yl]-6,7-dihydro-4*H*-pyrazolo[4,3-*c*]pyridin-5-yl]ethanone (3). To a solution of (S)-1-(3-bromo-1-(tetrahydrofuran-3-yl)-6,7-dihydro-1*H*-pyrazolo[4,3-*c*]pyridin-5(4*H*)-yl)ethanone (33, 300 mg, 0.96 mmol), 6-(1-methyl-1*H*-pyrazol-4-yl)-1,2,3,4-tetrahydroquinoline (39, 127 mg, 0.960 mmol), and *t*-BuONa (123 mg, 1.28 mmol) in 1,4-dioxane (3.0 mL) was added chloro(2-dicyclohexylphosphino-2',6'-di-*I*-propoxy-1,1'-biphenyl)[2-(2-aminoethylphenyl)]palladium(ii), methyl-*tert*-butylether adduct (78 mg, 0.096 mmol), and 2-dicyclohexylphosphino-2',6'-di-*I*-propoxy-1,1'-biphenyl (45 mg, 0.096 mmol). The mixture was heated to 120 °C for 12 h under a nitrogen atmosphere. After cooling the reaction to room temperature, the mixture was filtered and the filtrate was concentrated in vacuo. The crude residue was purified by reverse phase chromatography (acetone 38–68%/0.2% formic acid in water) to give the title compound (3, 145 mg, 34%) as a white solid. ¹H NMR (400 MHz, DMSO-*d*₆) δ 7.92 (s, 1H), 7.68 (s, 1H), 7.20 (s, 1H), 7.15–7.06 (m, 1H), 6.49–6.37 (m, 1H), 4.93–4.85 (m, 1H), 4.14–4.06 (m, 2H), 4.05–3.92 (m, 2H), 3.87–3.65 (m, 7H), 3.62–3.48 (m, 2H), 2.83–2.78 (m, 4H), 2.37–2.18 (m, 2H), 2.06–1.94 (m, 5H). LCMS *m/z* (M + H) 447.

1-[3-[7-(1-Methylpyrazol-4-yl)-2,3,4,5-tetrahydro-1-benzazepin-1-yl]-1-[(3*S*)-tetrahydrofuran-3-yl]-6,7-dihydro-4*H*-pyrazolo[4,3-*c*]pyridin-5-yl]ethanone (4). Step 1: (S)-1-(3-(2,3,4,5-Tetrahydro-1*H*-benzo[b]azepin-1-yl)-1-(tetrahydrofuran-3-yl)-6,7-dihydro-1*H*-pyrazolo[4,3-*c*]pyridin-5(4*H*)-yl)ethanone (42). To a solution of (S)-1-(3-bromo-1-(tetrahydrofuran-3-yl)-6,7-dihydro-1*H*-pyrazolo[4,3-*c*]pyridin-5(4*H*)-yl)ethanone (33, 500 mg, 1.6 mmol), 2,3,4,5-tetrahydro-1*H*-benzo[b]azepine (40, 235 mg, 1.60 mmol), and *t*-BuONa (461 mg, 4.80 mmol) in 1,4-dioxane (5.0 mL) was added chloro(2-dicyclohexylphosphino-2',6'-di-*i*-propoxy-1,1'-biphenyl)[2-(2-aminoethylphenyl)]palladium(ii), methyl-*tert*-butylether adduct (131 mg, 0.160 mmol) and 2-dicyclohexylphosphino-2',6'-di-*i*-propoxy-1,1'-biphenyl (75 mg, 0.16 mmol). The mixture was heated to 110 °C for 16 h under a nitrogen atmosphere. After cooling the reaction to room temperature, the mixture was filtered and the filtrate was concentrated in vacuo. The crude residue was purified by Prep-TLC (DCM/MeOH = 25:1) to give the presumed title compound (42, 400 mg, 60% purity) as a light-yellow solid.

Step 2: (S)-1-(3-(7-Bromo-2,3,4,5-tetrahydro-1*H*-benzo[b]azepin-1-yl)-1-(tetrahydrofuran-3-yl)-6,7-dihydro-1*H*-pyrazolo[4,3-*c*]pyridin-5(4*H*)-yl)ethanone (44). To a solution of (S)-1-(3-(2,3,4,5-tetrahydro-1*H*-benzo[b]azepin-1-yl)-1-(tetrahydrofuran-3-yl)-6,7-dihydro-1*H*-pyrazolo[4,3-*c*]pyridin-5(4*H*)-yl)ethanone (42, 400 mg, 60% purity) in DCM (3 mL) at 0 °C was added *N*-bromosuccinimide (154 mg, 0.860 mmol) portionwise. The mixture was stirred at room temperature for 16 h. The mixture was washed with water (40 mL \times 2).

The organic layer was dried over anhydrous Na_2SO_4 , filtered, and concentrated in vacuo. The crude residue was purified by silica gel chromatography (DCM/MeOH = 20:1) to give the title compound (**44**, 280 mg, 97%) as a yellow solid. LCMS m/z (M + H) 459.

Step 3: *1-[3-[7-(1-Methylpyrazol-4-yl)-2,3,4,5-tetrahydro-1-benzazepin-1-yl]-1-[(3S)-tetrahydrofuran-3-yl]-6,7-dihydro-4H-pyrazolo[4,3-c]pyridin-5-yl]ethanone (4).* To a solution of (S)-1-(3-(7-bromo-2,3,4,5-tetrahydro-1H-benzo[b]azepin-1-yl)-1-(tetrahydrofuran-3-yl)-6,7-dihydro-1H-pyrazolo[4,3-c]pyridin-5(4H)-yl)ethanone (**44**, 350 mg, 0.760 mmol) in dioxane (5 mL) and water (3 mL) was added 1-methyl-4-(4,4,5,5-tetramethyl-1,3,2-dioxaborolan-2-yl)-1H-pyrazole (175 mg, 0.840 mmol), K_2CO_3 (210 mg, 1.52 mmol) and [1,1'-bis(diphenylphosphino)ferrocene]dichloropalladium(II) (56 mg, 0.076 mmol). The mixture was heated to 110 °C for 18 h under a nitrogen atmosphere. After cooling the reaction to room temperature, the mixture was concentrated in vacuo. The residue was purified by reverse phase chromatography (acetonitrile 23–53%/0.2% formic acid in water) to give the title compound (**4**, 82 mg, 23%) as a white solid. ^1H NMR (400 MHz, DMSO- d_6) δ 8.06–8.05 (m, 1H), 8.00–7.79 (m, 1H), 7.44–7.42 (m, 1H), 7.31–7.26 (m, 1H), 6.90–6.77 (m, 1H), 4.81–4.78 (m, 1H), 4.03–3.98 (m, 2H), 3.84–3.78 (m, 5H), 3.55–3.43 (m, 6H), 2.77–2.55 (m, 4H), 2.25–2.22 (m, 2H), 1.97–1.62 (m, 7H). LCMS m/z (M + H) 483.

1-[3-[7-Methoxy-6-(1-methylpyrazol-4-yl)-3,4-dihydro-2H-quinolin-1-yl]-1-[(3S)-tetrahydrofuran-3-yl]-6,7-dihydro-4H-pyrazolo[4,3-c]pyridin-5-yl]ethanone (7). In a similar manner to **4**, compound **7** was prepared from 7-methoxy-1,2,3,4-tetrahydroquinoline (**41**) to provide the title compound (**7**, 24%) as a white solid. ^1H NMR (400 MHz, DMSO- d_6) δ 7.90 (s, 1H), 7.72 (s, 1H), 7.19 (s, 1H), 6.29 (s, 1H), 4.95–4.86 (m, 1H), 4.19–4.22 (m, 2H), 4.00–3.92 (m, 2H), 3.82–3.55 (m, 6H), 3.80 (s, 3H), 3.61 (s, 3H), 2.83–2.72 (m, 4H), 2.38–2.12 (m, 2H), 2.07–1.91 (m, 5H). LCMS m/z (M + H) 477.

1-[3-[7-Chloro-6-(1-methylpyrazol-4-yl)-3,4-dihydro-2H-quinolin-1-yl]-1-[(3S)-tetrahydrofuran-3-yl]-6,7-dihydro-4H-pyrazolo[4,3-c]pyridin-5-yl]ethanone (6). **Step 1:** *6-Bromo-7-chloro-1,2,3,4-tetrahydroquinoline (49).* To a solution of 7-chloro-1,2,3,4-tetrahydroquinoline (**46**, 14 g, 80 mmol) in DCM (100 mL) at 0 °C was added *N*-bromosuccinimide (14.8 g, 80.0 mmol). The mixture was stirred at room temperature for 1 h. Water (100 mL) was added, and the mixture was extracted with DCM (100 mL \times 2). The combined organic layers were dried over anhydrous Na_2SO_4 , filtered, and concentrated in vacuo. The crude residue was purified by silica gel chromatography (petroleum ether/EtOAc = 100:1) to give the title compound (**49**, 7.1 g, 36%) as a light-yellow solid. LCMS m/z (M + H) 246.

Step 2: *7-Chloro-6-(1-methyl-1H-pyrazol-4-yl)-1,2,3,4-tetrahydroquinoline (52).* To a solution of 6-bromo-7-chloro-1,2,3,4-tetrahydroquinoline (**49**, 2.1 g, 8.5 mmol) in dioxane/H₂O (60 mL, 5:1) was added 1-methyl-4-(4,4,5,5-tetramethyl-1,3,2-dioxaborolan-2-yl)-1H-pyrazole (1.9 g, 9.4 mmol), Na_2CO_3 (1.8 g, 17 mmol), and [1,1'-bis(diphenylphosphino)ferrocene]dichloropalladium(II) (622 mg, 0.900 mmol). The mixture was heated to 110 °C for 12 h under a nitrogen atmosphere. After cooling the reaction to room temperature, the mixture was concentrated in vacuo. The crude residue was purified by silica gel chromatography (petroleum ether/EtOAc = 4:1) to give the title compound (**52**, 2.0 g, 95%) as yellow solid. ^1H NMR (400 MHz, DMSO- d_6) δ 7.88–7.85 (m, 1H), 7.61 (s, 1H), 7.01 (s, 1H), 6.53 (s, 1H), 5.95 (s, 1H), 3.86–3.84 (m, 3H), 3.38–3.16 (m, 2H), 2.65–2.62 (m, 2H), 1.80–1.74 (m, 2H).

Step 3: *1-[3-[7-Chloro-6-(1-methylpyrazol-4-yl)-3,4-dihydro-2H-quinolin-1-yl]-1-[(3S)-tetrahydrofuran-3-yl]-6,7-dihydro-4H-pyrazolo[4,3-c]pyridin-5-yl]ethanone (6).* To a solution of 7-chloro-6-(1-methyl-1H-pyrazol-4-yl)-1,2,3,4-tetrahydroquinoline (**52**, 247 mg, 1.0 mmol) in dioxane (3 mL) and toluene (3 mL) was added *t*-BuONa (288 mg, 3.00 mmol), tris(dibenzylideneacetone)dipalladium (46 mg, 0.050 mmol), 4,5-bis(diphenylphosphino)-9,9-dimethylxanthene (59 mg, 0.10 mmol), and (S)-1-(3-bromo-1-(tetrahydrofuran-3-yl)-6,7-dihydro-1H-pyrazolo[4,3-c]pyridin-5(4H)-yl)ethanone (**33**, 313 mg, 1.00 mmol). The mixture was heated to 90 °C for 16 h under a nitrogen atmosphere. After cooling the reaction to room temperature, the mixture was concentrated in vacuo. The crude residue was purified by silica gel chromatography (petroleum ether/EtOAc = 40:1) to give the title compound (**53**, 520 mg, 86%) as yellow oil. LCMS m/z (M + H) 264.

Prep-TLC (DCM/MeOH = 20:1) to give the title compound (**6**, 240 mg, 50%) as a light-yellow solid. ^1H NMR (400 MHz, DMSO- d_6) δ 7.97 (s, 1H), 7.68 (s, 1H), 7.21–7.20 (m, 1H), 6.54–6.50 (m, 1H), 4.95–4.89 (m, 1H), 4.18–4.15 (m, 2H), 4.03–3.98 (m, 2H), 3.85–3.71 (m, 7H), 3.54–3.50 (m, 2H), 2.86–2.77 (m, 4H), 2.33–2.27 (m, 2H), 2.08–1.94 (m, 5H). LCMS m/z (M + H) 481.

1-[3-[7-(Difluoromethyl)-6-(1-methylpyrazol-4-yl)-3,4-dihydro-2H-quinolin-1-yl]-1-[(3S)-tetrahydrofuran-3-yl]-6,7-dihydro-4H-pyrazolo[4,3-c]pyridin-5-yl]ethanone (8). **Step 1:** *Quinoline-7-carbaldehyde.* To a solution of 7-methylquinoline (27.0 g, 189 mmol) at 160 °C was added SeO_2 (21.0 g, 189 mmol) portionwise over 5 min. The mixture was stirred at 160 °C for 8 h. After cooling the reaction to room temperature, DCM (400 mL) was added and the mixture was filtered through Celite. The organic layer was concentrated in vacuo. The crude residue was purified by silica gel chromatography (petroleum ether/EtOAc = 10:1) to give the title compound (14.0 g, 47%) as yellow oil. ^1H NMR (400 MHz, CDCl_3) δ 10.23 (s, 1H), 9.03 (d, J = 2.8 Hz, 1H), 8.56 (s, 1H), 8.22 (d, J = 8.4 Hz, 1H), 8.04 (d, J = 8.4 Hz, 1H), 7.93 (d, J = 8.4 Hz, 1H), 7.55–7.52 (m, 1H).

Step 2: *7-(Difluoromethyl)quinoline.* To a solution of quinoline-7-carbaldehyde (14.0 g, 89.2 mmol) in DCM (150 mL) 0 °C was added diethylaminosulfur trifluoride (65.0 g, 446 mmol) dropwise over 20 min. The mixture was stirred at room temperature for 16 h. The mixture was poured into satd aq NaHCO_3 (1 L) at 0 °C and extracted with DCM (200 mL \times 2). The combined organic layers were dried over anhydrous Na_2SO_4 , filtered, and concentrated in vacuo. The crude residue was purified by silica gel chromatography (petroleum ether/EtOAc = 5:1) to give the title compound (13.0 g, 81%) as yellow oil. ^1H NMR (400 MHz, CDCl_3) δ 8.92 (d, J = 2.8 Hz, 1H), 8.15 (d, J = 8.4 Hz, 2H), 7.86 (d, J = 8.4 Hz, 1H), 7.63 (d, J = 8.8 Hz, 1H), 7.44–7.41 (m, 1H), 6.78 (t, J = 56.0 Hz, 1H).

Step 3: *7-(Difluoromethyl)-1,2,3,4-tetrahydroquinoline (47).* To a solution of 7-(difluoromethyl)quinoline (13.0 g, 72.6 mmol) and NaBH_3CN (23.0 g, 363 mmol) in MeOH (150 mL) at 0 °C was added boron trifluoride diethyl etherate (17.9 mL, 145 mmol) dropwise over 20 min. The mixture was heated to 90 °C for 24 h. After cooling the reaction to room temperature, the mixture was poured into satd aq NaHCO_3 (1 L) at 0 °C and extracted with DCM (200 mL \times 2). The combined organic layers were dried over Na_2SO_4 , filtered, and concentrated in vacuo. The crude residue was purified by silica gel chromatography (petroleum ether/EtOAc = 20:1) to give the title compound (47, 8.0 g, 56%) as brown oil. ^1H NMR (400 MHz, CDCl_3) δ 7.00 (d, J = 7.2 Hz, 1H), 6.71 (d, J = 8.0 Hz, 1H), 6.59 (s, 1H), 6.50 (t, J = 56.8 Hz, 1H), 3.33 (t, J = 5.6 Hz, 2H), 2.79 (t, J = 6.4 Hz, 2H), 1.98–1.92 (m, 2H).

Step 4: *6-Bromo-7-(difluoromethyl)-1,2,3,4-tetrahydroquinoline (50).* To a solution of 7-(difluoromethyl)-1,2,3,4-tetrahydroquinoline (47, 7.00 g, 38.3 mmol) in DCM (100 mL) at 0 °C was added *N*-bromosuccinimide (6.90 g, 38.3 mmol) portionwise over 20 min. The mixture was stirred at room temperature for 16 h. The mixture was poured into water (100 mL) and extracted with DCM (200 mL \times 2). The combined organic layers were dried over Na_2SO_4 , filtered, and concentrated in vacuo. The crude residue was purified by silica gel chromatography (petroleum ether/EtOAc = 300:1) to give the title compound (50, 6.0 g, 60%) as light-yellow oil. ^1H NMR (400 MHz, CDCl_3) δ 7.13 (s, 1H), 6.78 (t, J = 55.2 Hz, 1H), 6.72 (s, 1H), 3.31 (t, J = 5.2 Hz, 2H), 2.74 (t, J = 6.0 Hz, 2H), 1.95–1.87 (m, 2H).

Step 5: *7-(Difluoromethyl)-6-(1-methyl-1H-pyrazol-4-yl)-1,2,3,4-tetrahydroquinoline (53).* To a solution of 6-bromo-7-(difluoromethyl)-1,2,3,4-tetrahydroquinoline (50, 600 mg, 2.30 mmol) in dioxane (8 mL) and H_2O (2 mL) was added K_2CO_3 (635 mg, 4.6 mmol), [1,1'-bis(diphenylphosphino)ferrocene]dichloropalladium(II) (169 mg, 0.23 mmol), and 1-methyl-4-(4,4,5,5-tetramethyl-1,3,2-dioxaborolan-2-yl)-1H-pyrazole (478 mg, 2.30 mmol). The mixture was heated to 110 °C for 18 h under a nitrogen atmosphere. After cooling the reaction to room temperature, the mixture was concentrated in vacuo. The crude residue was purified by silica gel chromatography (petroleum ether/EtOAc = 40:1) to give the title compound (53, 520 mg, 86%) as yellow oil. LCMS m/z (M + H) 264.

Step 6: 1-[3-[7-(Difluoromethyl)-6-(1-methylpyrazol-4-yl)-3,4-dihydro-2H-quinolin-1-yl]-1-tetrahydrofuran-3-yl]-6,7-dihydro-4H-pyrazolo[4,3-c]pyridin-5-yl]ethanone. To a solution of 1-(3-bromo-1-(tetrahydrofuran-3-yl)-6,7-dihydro-1H-pyrazolo[4,3-c]pyridin-5(4H)-yl)ethanone (32, 313 mg, 1.0 mmol), 7-(difluoromethyl)-6-(1-methyl-1H-pyrazol-4-yl)-1,2,3,4-tetrahydroquinoline (53, 263 mg, 1.0 mmol), and *t*-BuONa (288 mg, 3.0 mmol) in 1,4-dioxane (10 mL) was added chloro(2-dicyclohexylphosphino-2',6'-di-i-propoxy-1,1'-biphenyl)[2-(2-aminoethylphenyl)]palladium(II), methyl-*tert*-butylether adduct (82 mg, 0.10 mmol), and 2-dicyclohexylphosphino-2',6'-di-*I*-propoxy-1,1'-biphenyl (47 mg, 0.10 mmol). The mixture was irradiated in a microwave at 130 °C for 45 min. After cooling to room temperature, the mixture was filtered and the filtrate was concentrated in vacuo. The crude residue was purified by Prep-TLC (DCM/MeOH = 20:1) to give the title compound (76 mg, 16%) as a light-yellow solid. ¹H NMR (400 MHz, DMSO-*d*₆) δ 7.76 (s, 1H), 7.50 (s, 1H), 7.11 (s, 1H), 6.94–6.65 (m, 2H), 4.94–4.88 (m, 1H), 4.16–4.12 (m, 2H), 4.03–3.90 (m, 2H), 3.86 (s, 3H), 3.82–3.79 (m, 4H), 3.70–3.56 (m, 2H), 2.86–2.74 (m, 4H), 2.29–2.22 (m, 2H), 2.07–1.96 (m, 5H). LCMS *m/z* (M + H) 497.

Step 7: 1-[3-[7-(Difluoromethyl)-6-(1-methylpyrazol-4-yl)-3,4-dihydro-2H-quinolin-1-yl]-1-[(3*S*)-tetrahydrofuran-3-yl]-6,7-dihydro-4H-pyrazolo[4,3-c]pyridin-5-yl]ethanone (8). Racemic 1-[3-[7-(difluoromethyl)-6-(1-methylpyrazol-4-yl)-3,4-dihydro-2H-quinolin-1-yl]-1-tetrahydrofuran-3-yl]-6,7-dihydro-4H-pyrazolo[4,3-c]pyridin-5-yl]ethanone (50 mg) was separated by using chiral SFC (cellulose-3 150 mm × 21.2 mm I.D.; Supercritical CO₂/MeOH (0.1% NH₄OH) = 20/80 at 70 mL/min) to give 1-[3-[7-(difluoromethyl)-6-(1-methylpyrazol-4-yl)-3,4-dihydro-2H-quinolin-1-yl]-1-[(3*R*)-tetrahydrofuran-3-yl]-6,7-dihydro-4H-pyrazolo[4,3-c]pyridin-5-yl]ethanone (22 mg, second peak) and 1-[3-[7-(difluoromethyl)-6-(1-methylpyrazol-4-yl)-3,4-dihydro-2H-quinolin-1-yl]-1-[(3*S*)-tetrahydrofuran-3-yl]-6,7-dihydro-4H-pyrazolo[4,3-c]pyridin-5-yl]ethanone (8, 17 mg, first peak). *R*-isomer: ¹H NMR (400 MHz, DMSO-*d*₆) δ 7.75 (s, 1H), 7.51 (s, 1H), 7.11 (s, 1H), 6.94–6.64 (m, 2H), 4.95–4.88 (m, 1H), 4.17–4.12 (m, 2H), 4.04–3.91 (m, 2H), 3.86 (s, 3H), 3.82–3.80 (m, 4H), 3.70–3.56 (m, 2H), 2.87–2.74 (m, 4H), 2.29–2.22 (m, 2H), 2.07–1.97 (m, 5H). LCMS *m/z* (M + H) 497. *S*-isomer (8): ¹H NMR (400 MHz, DMSO-*d*₆) δ 7.76 (s, 1H), 7.49 (s, 1H), 7.10 (s, 1H), 6.93–6.64 (m, 2H), 4.94–4.88 (m, 1H), 4.16–4.12 (m, 2H), 4.03–3.90 (m, 2H), 3.86 (s, 3H), 3.82–3.79 (m, 4H), 3.69–3.56 (m, 2H), 2.86–2.73 (m, 4H), 2.30–2.20 (m, 2H), 2.06–1.96 (m, 5H). LCMS *m/z* (M + H) 497.

1-[3-[6-(1-Methylpyrazol-4-yl)-7-(trifluoromethyl)-3,4-dihydro-2H-quinolin-1-yl]-1-[(3*S*)-tetrahydrofuran-3-yl]-6,7-dihydro-4H-pyrazolo[4,3-c]pyridin-5-yl]ethanone (9). **Step 1:** 6-Bromo-7-(trifluoromethyl)-1,2,3,4-tetrahydroquinoline (51). To a solution of 7-(trifluoromethyl)-1,2,3,4-tetrahydroquinoline (48, 800 mg, 3.98 mmol) in DCM (50 mL) at 0 °C was added *N*-bromosuccinimide (637 mg, 3.58 mmol) portionwise over 20 min. The mixture was stirred at room temperature for 1 h. The reaction was concentrated in vacuo. The crude residue was purified by silica gel chromatography (petroleum ether/EtOAc = 10:1) to give the presumed title compound (51, 430 mg, 39%) as yellow oil.

Step 2: 6-(1-Methyl-1H-pyrazol-4-yl)-7-(trifluoromethyl)-1,2,3,4-tetrahydroquinoline (54). To a solution of 6-bromo-7-(trifluoromethyl)-1,2,3,4-tetrahydroquinoline (51, 430 mg, 1.54 mmol) in dioxane (20 mL) and H₂O (4 mL) was added Na₂CO₃ (488 mg, 4.61 mmol), chloro(2-dicyclohexylphosphino-2',4',6'-tri-*i*-propyl-1,1'-biphenyl)(2'-amino-1,1'-biphenyl-2-yl)palladium(II) (121 mg, 0.150 mmol), 2-(dicyclohexylphosphino)-2',4',6'-trisopropylbiphenyl (73 mg, 0.15 mmol), and 1-methyl-4-(4,4,5,5-tetramethyl-1,3,2-dioxaborolan-2-yl)-1H-pyrazole (383 mg, 1.84 mmol). The mixture was heated to 80 °C for 3 h under a nitrogen atmosphere. After cooling to room temperature, the mixture was concentrated in vacuo. The crude residue was purified by silica gel chromatography (petroleum ether/EtOAc = 3:1) to give the presumed title compound (54, 300 mg, 70%) as a white solid.

Step 3: 1-[3-[6-(1-Methylpyrazol-4-yl)-7-(trifluoromethyl)-3,4-dihydro-2H-quinolin-1-yl]-1-[(3*S*)-tetrahydrofuran-3-yl]-6,7-dihydro-4H-pyrazolo[4,3-c]pyridin-5-yl]ethanone (9). To a solution of (S)-1-(3-bromo-1-(tetrahydrofuran-3-yl)-6,7-dihydro-1H-pyrazolo[4,3-c]pyridin-5(4H)-yl)ethanone (33, 112 mg, 0.360 mmol), 6-(1-methyl-1H-pyrazol-4-yl)-7-(trifluoromethyl)-1,2,3,4-tetrahydroquinoline (54,

100 mg, 0.36 mmol), and *t*-BuONa (103 mg, 1.07 mmol) in 1,4-dioxane (2 mL) was added dichloro[1,3-bis(2,6-di-3-pentylphenyl)-imidazol-2-ylidene](3-chloropyridyl)palladium(II) (28 mg, 0.040 mmol). The mixture was irradiated in a microwave at 150 °C for 1 h. After cooling to room temperature, water (40 mL) was added and extracted with EtOAc (30 mL × 3). The combined organic layers were washed with brine (50 mL), dried over anhydrous Na₂SO₄, filtered, and concentrated in vacuo. The crude residue was purified by reverse phase chromatography (acetonitrile 40–70%/0.225% formic acid in water) to give the title compound (9, 39 mg, 21%) as a white solid. ¹H NMR (400 MHz, CDCl₃) δ 7.53 (d, *J* = 2.8 Hz, 1H), 7.41 (d, *J* = 7.2 Hz, 1H), 7.07–7.02 (m, 1H), 6.90 (d, *J* = 7.6 Hz, 1H), 4.78–4.76 (m, 1H), 4.27–4.13 (m, 4H), 4.00–3.91 (m, 3H), 3.93 (s, 3H), 3.76–3.70 (m, 3H), 2.88–2.84 (m, 4H), 2.43–2.39 (m, 2H), 2.18–2.06 (m, 5H). LCMS *m/z* (M + H) 515.

1-[3-[7-Methyl-6-(1-methylpyrazol-4-yl)-3,4-dihydro-2H-quinolin-1-yl]-1-[(3*S*)-tetrahydrofuran-3-yl]-6,7-dihydro-4H-pyrazolo[4,3-c]pyridin-5-yl]ethanone (5). To a solution of 1-[3-[7-chloro-6-(1-methylpyrazol-4-yl)-3,4-dihydro-2H-quinolin-1-yl]-1-[(3*S*)-tetrahydrofuran-3-yl]-6,7-dihydro-4H-pyrazolo[4,3-c]pyridin-5-yl]ethanone (6, 150 mg, 0.313 mmol) in toluene (3 mL) and H₂O (1 mL) was added MeBF₃K (116 mg, 0.939 mmol), palladium(II) acetate (7 mg, 0.03 mmol), Cs₂CO₃ (612 mg, 0.626 mmol), and di(adamantan-1-yl)(butyl)phosphine (23 mg, 0.0616 mmol). The mixture was heated to 100 °C for 18 h under a nitrogen atmosphere. After cooling the reaction to room temperature, the mixture was concentrated in vacuo. The crude residue was purified by Prep-TLC (DCM/MeOH = 20:1) to give the title compound (5, 21 mg, 15%) as a white solid. ¹H NMR (400 MHz, DMSO-*d*₆) δ 7.76 (s, 1H), 7.52 (s, 1H), 6.99–6.98 (m, 1H), 6.36–6.34 (m, 1H), 4.90–4.85 (m, 1H), 4.14–4.05 (m, 2H), 4.04–3.93 (m, 2H), 3.87–3.66 (m, 7H), 3.58–3.52 (m, 2H), 2.84–2.67 (m, 4H), 2.34–2.21 (m, 2H), 2.15 (s, 3H), 2.09–1.81 (m, 5H). LCMS *m/z* (M + H) 461.

1-(3-[7-(Difluoromethyl)-6-(1-methyl-1H-pyrazol-4-yl)-3,4-dihydroquinolin-1(2H)-yl]-1-(tetrahydro-2H-pyran-4-yl)-1,4,6,7-tetrahydro-5H-pyrazolo[4,3-c]pyridin-5-yl)ethanone (10). To a solution of 7-(difluoromethyl)-6-(1-methyl-1H-pyrazol-4-yl)-1,2,3,4-tetrahydroquinoline (53, 251 mg, 0.950 mmol) in 2-methyl-2-butanol (8 mL) was added 1-(3-bromo-1-(tetrahydro-2H-pyran-4-yl)-6,7-dihydro-1H-pyrazolo[4,3-c]pyridin-5(4H)-yl)ethanone (34, 500 mg, 1.52 mmol), (2-dicyclohexylphosphino-2,4,6-triisopropyl-1,1-biphenyl)[2-(2-amino-1,1-biphenyl)]palladium(II) methanesulfonate (129 mg, 0.150 mmol), and K₃PO₄ (971 mg, 4.60 mmol). The mixture was heated to 95 °C for 42 h under an argon atmosphere. After cooling the reaction to room temperature, the mixture was concentrated in vacuo. The crude residue was purified by silica gel chromatography (DCM/MeOH = 50:1) to give 1-[3-[7-(difluoromethyl)-6-(1-methyl-pyrazol-4-yl)-3,4-dihydro-2H-quinolin-1-yl]-1-tetrahydrofuran-3-yl]-6,7-dihydro-4H-pyrazolo[4,3-c]pyridin-5-yl]ethanone (10, 360 mg, 74%) as a yellow solid. ¹H NMR (400 MHz, DMSO-*d*₆) δ 7.75 (s, 1H), 7.50 (s, 1H), 7.10 (s, 1H), 6.96–6.63 (m, 2H), 4.33–4.25 (m, 1H), 4.20–4.09 (m, 2H), 3.99–3.90 (m, 2H), 3.86 (s, 3H), 3.78–3.66 (m, 2H), 3.63–3.55 (m, 2H), 3.49–3.41 (m, 2H), 2.89–2.66 (m, 4H), 2.11–1.90 (m, 7H), 1.85–1.80 (m, 2H). ¹³C NMR (101 MHz, 360 K, DMSO-*d*₆) δ 169.3, 148.4, 142.7, 138.3, 137.7, 131.1, 129.7, 129.2 (*t*, *J* = 20.8 Hz), 126.4, 121.4, 119.1, 114.3 (*t*, *J* = 235.3 Hz), 110.7, 106.5, 66.5, 54.5, 49.6, 43.4, 39.0, 38.7, 32.8, 27.4, 22.5, 22.3, 21.7; HRMS *m/z* 511.2628 (M + H⁺, C₂₇H₃₃F₂N₆O₂ requires 511.2633).

1-[1-Cyclohexyl-3-[7-(difluoromethyl)-6-(1-methylpyrazol-4-yl)-3,4-dihydro-2H-quinolin-1-yl]-6,7-dihydro-4H-pyrazolo[4,3-c]pyridin-5-yl]ethanone (11). **Step 1:** *tert*-Butyl 3-Bromo-1-((2-(trimethylsilyl)ethoxy)methyl)-6,7-dihydro-1H-pyrazolo[4,3-c]pyridine-5(4H)-carboxylate (**55**) and *tert*-Butyl 3-Bromo-2-((2-(trimethylsilyl)ethoxy)methyl)-6,7-dihydro-2H-pyrazolo[4,3-c]pyridine-5(4H)-carboxylate. To a solution of *tert*-butyl 3-bromo-6,7-dihydro-1H-pyrazolo[4,3-c]pyridine-5(4H)-carboxylate (**26**, 80.0 g, 265 mmol) in THF (1.5 L) at 0 °C was added sodium hydride (60%, 12.71 g, 317.7 mmol) portionwise. The mixture was stirred at room temperature for 0.5 h. 2-(Trimethylsilyl)ethoxymethyl chloride (52.97 g, 317.7 mmol) was added dropwise and the mixture stirred at room temperature for an additional 16 h. The mixture was quenched with water (1 L) and

extracted with EtOAc (500 mL \times 3). The combined organic layers were dried over anhydrous Na₂SO₄, filtered, and concentrated in vacuo. The crude residue was purified by silica gel chromatography (petroleum ether/EtOAc = 5:1) to give a mixture of the title compounds (**55**, 95 g, 83%) as yellow oil. LCMS *m/z* (M + H) 434.

Step 2: *tert*-Butyl 3-(7-(difluoromethyl)-6-(1-methyl-1*H*-pyrazol-4-yl)-3,4-dihydroquinolin-1(2*H*)-yl)-1-((2-(trimethylsilyl)ethoxy)methyl)-6,7-dihydro-1*H*-pyrazolo[4,3-*c*]pyridine-5(4*H*)-carboxylate (**56**). To a solution of *tert*-butyl 3-bromo-1-((2-(trimethylsilyl)ethoxy)methyl)-6,7-dihydro-1*H*-pyrazolo[4,3-*c*]pyridine-5(4*H*)-carboxylate and *tert*-butyl 3-bromo-2-((2-(trimethylsilyl)ethoxy)methyl)-6,7-dihydro-2*H*-pyrazolo[4,3-*c*]pyridine-5(4*H*)-carboxylate (**55**, 65.7 g, 152 mmol) in 1,4-dioxane (200 mL) was added chloro(2-dicyclohexylphosphino-2',6'-di-i-propoxy-1,1'-biphenyl)(2'-amino-1,1'-biphenyl-2-yl)palladium(II) (5.9 g, 7.6 mmol), 2-dicyclohexylphosphino-2',6'-di-i-propoxy-1,1'-biphenyl (3.54 g, 7.6 mmol), 7-(difluoromethyl)-6-(1-methyl-1*H*-pyrazol-4-yl)-1,2,3,4-tetrahydroquinoline (20 g, 75.96 mmol), and *t*-BuONa (21.9 g, 227.89 mmol). The mixture was heated to 120 °C for 16 h under an argon atmosphere. After cooling the reaction to room temperature, water (800 mL) was added and extracted with EtOAc (500 mL \times 3). The combined organic layers were washed with brine (500 mL \times 3), dried over anhydrous Na₂SO₄, filtered, and concentrated in vacuo. The crude residue was purified by silica gel chromatography (DCM/MeOH = 50:1) to give the title compound (**56**, 9.1 g, 20%) as a yellow oil. ¹H NMR (400 MHz, CDCl₃) δ 7.54 (s, 1H), 7.41 (s, 1H), 7.03 (s, 1H), 6.88 (s, 1H), 6.52 (t, *J* = 55.6 Hz, 1H), 5.33 (s, 2H), 4.10 (s, 2H), 3.96 (s, 3H), 3.73–3.70 (m, 4H), 3.64 (t, *J* = 8.0 Hz, 2H), 2.87–2.80 (m, 4H), 2.09–2.07 (m, 2H), 1.45 (s, 9H), 0.93 (t, *J* = 8.0 Hz, 2H), 0.00 (s, 9H). LCMS *m/z* (M + H) 615.

Step 3: *tert*-Butyl 3-(7-(difluoromethyl)-6-(1-methyl-1*H*-pyrazol-4-yl)-3,4-dihydroquinolin-1(2*H*)-yl)-6,7-dihydro-1*H*-pyrazolo[4,3-*c*]pyridine-5(4*H*)-carboxylate (**57**). To a solution of *tert*-butyl 3-(7-(difluoromethyl)-6-(1-methyl-1*H*-pyrazol-4-yl)-3,4-dihydroquinolin-1(2*H*)-yl)-1-((2-(trimethylsilyl)ethoxy)methyl)-6,7-dihydro-1*H*-pyrazolo[4,3-*c*]pyridine-5(4*H*)-carboxylate (**56**, 8.5 g, 14 mmol) in THF (50 mL) was added tetrabutylammonium fluoride (1.0 M in THF, 40 mL, 40 mmol). The mixture was heated to 60 °C for 16 h under a nitrogen atmosphere. After cooling the reaction to room temperature, EtOAc (200 mL) was added and washed with brine (100 mL \times 3). The organic layer was dried over anhydrous Na₂SO₄, filtered, and concentrated in vacuo. The crude residue was purified by silica gel chromatography (DCM/MeOH = 20:1) to give the title compound (**57**, 4.4 g, 66%) as a yellow solid. ¹H NMR (400 MHz, CDCl₃) δ 7.54 (s, 1H), 7.42 (s, 1H), 7.03 (s, 1H), 6.87 (s, 1H), 6.52 (t, *J* = 55.6 Hz, 1H), 4.12 (s, 2H), 3.96 (s, 3H), 3.72–3.69 (m, 4H), 2.86–2.76 (m, 4H), 2.08–2.05 (m, 2H), 1.45 (s, 9H). LCMS *m/z* (M + H) 485.

Step 4: 7-(difluoromethyl)-6-(1-methyl-1*H*-pyrazol-4-yl)-1-(4,5,6,7-tetrahydro-1*H*-pyrazolo[4,3-*c*]pyridin-3-yl)-1,2,3,4-tetrahydroquinoline (**58**). To a solution of *tert*-butyl 3-(7-(difluoromethyl)-6-(1-methyl-1*H*-pyrazol-4-yl)-3,4-dihydroquinolin-1(2*H*)-yl)-6,7-dihydro-1*H*-pyrazolo[4,3-*c*]pyridine-5(4*H*)-carboxylate (**57**, 2.0 g, 4.13 mmol) in DCM (5 mL) at 0 °C was added trifluoroacetic acid (4.0 mL, 4.13 mmol). The mixture was stirred at 20 °C for 16 h and concentrated in vacuo to give the title compound (**58**, 2.0 g, crude) as brown oil that required no further purification. LCMS *m/z* (M + H) 385.

Step 5: 1-[3-(7-(difluoromethyl)-6-(1-methyl-1*H*-pyrazol-4-yl)-3,4-dihydro-2*H*-quinolin-1-yl]-1,4,6,7-tetrahydropyrazolo[4,3-*c*]pyridin-5-yl]ethanone (**59**). To a solution of 7-(difluoromethyl)-6-(1-methyl-1*H*-pyrazol-4-yl)-1-(4,5,6,7-tetrahydro-1*H*-pyrazolo[4,3-*c*]pyridin-3-yl)-1,2,3,4-tetrahydroquinoline (**58**, 120 mg, 0.310 mmol) in DCM (5 mL) at 0 °C was added triethylamine (0.09 mL, 0.6 mmol) and acetic anhydride (0.04 mL, 0.62 mmol). The mixture was stirred at 20 °C for 1 h. DCM (50 mL) was added and washed with water (30 mL \times 3) and brine (30 mL). The organic layer was dried over anhydrous Na₂SO₄, filtered, and concentrated in vacuo. The crude residue was purified by reverse phase chromatography (acetone/nitrobenzene 26–56%/0.05% NH₄OH in water) to give the title compound (**59**, 19 mg, 14%) as a white solid. ¹H NMR (400 MHz, DMSO-*d*₆) δ 12.42–12.31 (m, 1H), 7.75 (s, 1H), 7.50 (s, 1H), 7.10 (s, 1H), 6.96–6.62 (m, 1H), 6.73 (s, 1H), 4.21–4.04 (m,

2H), 3.86 (s, 3H), 3.76–3.51 (m, 4H), 2.88–2.66 (m, 4H), 2.07–1.87 (m, 5H). LCMS *m/z* (M + H) 427.

Step 6: 1-[1-Cyclohexyl-3-[7-(difluoromethyl)-6-(1-methylpyrazol-4-yl)-3,4-dihydro-2*H*-quinolin-1-yl]-6,7-dihydro-4*H*-pyrazolo[4,3-*c*]pyridin-5-yl]ethanone (**11**). To a solution of 1-[3-[7-(difluoromethyl)-6-(1-methylpyrazol-4-yl)-3,4-dihydro-2*H*-quinolin-1-yl]-1,4,6,7-tetrahydropyrazolo[4,3-*c*]pyridin-5-yl]ethanone (**59**, 50 mg, 0.12 mmol) in DMF (5 mL) was added Cs₂CO₃ (69 mg, 0.21 mmol) and bromocyclohexane (0.03 mL, 0.23 mmol). The mixture was heated to 80 °C for 24 h. After cooling to room temperature, the mixture was filtered and concentrated in vacuo. The crude residue was purified by reverse phase chromatography (acetone/nitrobenzene 42–72%/0.2% formic acid in water) to give the title compound (**11**, 3 mg, 5%) as a white solid. ¹H NMR (400 MHz, CDCl₃) δ 7.52 (d, *J* = 5.6 Hz, 1H), 7.40 (d, *J* = 6.4 Hz, 1H), 7.06–6.96 (m, 1H), 6.86 (d, *J* = 2.4 Hz, 1H), 6.68–6.34 (m, 1H), 4.30–4.10 (m, 2H), 3.96 (s, 3H), 3.92–3.83 (m, 2H), 3.76–3.66 (m, 3H), 2.90–2.72 (m, 4H), 2.19–2.02 (m, 7H), 1.96–1.88 (m, 6H), 1.44–1.22 (m, 2H). LCMS *m/z* (M + H) 509.

1-[3-[7-(difluoromethyl)-6-(1-methylpyrazol-4-yl)-3,4-dihydro-2*H*-quinolin-1-yl]-1-(1-methylsulfonyl-4-piperidyl)-6,7-dihydro-4*H*-pyrazolo[4,3-*c*]pyridin-5-yl]ethanone (15**). In a similar manner to **11**, compound **15** was prepared from 1-(methylsulfonyl)-piperidin-4-yl methanesulfonate to provide the title compound (**15**, 7%). ¹H NMR (400 MHz, CDCl₃) δ 7.57–7.54 (m, 1H), 7.44–7.39 (m, 1H), 7.07–7.01 (m, 1H), 6.90–6.87 (m, 1H), 6.71–6.37 (m, 1H), 4.28–4.13 (m, 2H), 4.10–4.02 (m, 1H), 3.99–3.91 (m, 3H), 3.96 (s, 3H), 3.75–3.69 (m, 3H), 3.02–2.92 (m, 2H), 2.90–2.83 (m, 5H), 2.81–2.71 (m, 2H), 2.39–2.24 (m, 2H), 2.17–2.05 (m, 7H). LCMS *m/z* (M + H) 588.**

1-[3-[7-(difluoromethyl)-6-(1-methylpyrazol-4-yl)-3,4-dihydro-2*H*-quinolin-1-yl]-1-(4-piperidyl)-6,7-dihydro-4*H*-pyrazolo[4,3-*c*]pyridin-5-yl]ethanone (13**). Step 1: *tert*-Butyl 4-(5-Acetyl-3-(7-(difluoromethyl)-6-(1-methyl-1*H*-pyrazol-4-yl)-3,4-dihydroquinolin-1(2*H*)-yl)-4,5,6,7-tetrahydro-1*H*-pyrazolo[4,3-*c*]pyridin-1-yl)-piperidine-1-carboxylate (**60**). In a similar manner to **11**, compound **60** was prepared from *tert*-butyl 4-((methylsulfonyl)oxy)piperidin-1-carboxylate to provide the title compound (**60**, 17%) as a white solid. ¹H NMR (400 MHz, CDCl₃) δ 7.55–7.53 (m, 1H), 7.42–7.40 (m, 1H), 7.06–7.00 (m, 1H), 6.86 (s, 1H), 6.68–6.37 (m, 1H), 4.38–4.12 (m, 3H), 4.08–3.99 (m, 1H), 3.96 (s, 3H), 3.95–3.89 (m, 2H), 3.75–3.67 (m, 3H), 2.89–2.70 (m, 6H), 2.17–2.03 (m, 7H), 1.92–1.88 (m, 2H), 1.48 (s, 9H). LCMS *m/z* (M + H) 610.**

Step 2: 1-[3-[7-(difluoromethyl)-6-(1-methylpyrazol-4-yl)-3,4-dihydro-2*H*-quinolin-1-yl]-1-(4-piperidyl)-6,7-dihydro-4*H*-pyrazolo[4,3-*c*]pyridin-5-yl]ethanone (**12**). To a solution of *tert*-butyl 4-(5-acetyl-3-(7-(difluoromethyl)-6-(1-methyl-1*H*-pyrazol-4-yl)-3,4-dihydroquinolin-1(2*H*)-yl)-4,5,6,7-tetrahydro-1*H*-pyrazolo[4,3-*c*]pyridin-1-yl)piperidine-1-carboxylate (**60**, 50 mg, 0.090 mmol) in DCM (2 mL) at 0 °C was added trifluoroacetic acid (0.07 mL, 0.9 mmol). The mixture was stirred at room temperature for 1 h and concentrated in vacuo. The mixture was diluted with DCM (10 mL) and washed with satd aq NaHCO₃ (10 mL \times 2) and brine (10 mL). The organic layer was dried over anhydrous Na₂SO₄, filtered, and concentrated in vacuo. The crude residue was resolved in MeOH (1 mL), water added (10 mL), and lyophilized to give the title compound (**12**, 22 mg, 49%) as a white solid. ¹H NMR (400 MHz, CDCl₃) δ 7.54 (d, *J* = 6.0 Hz, 1H), 7.41 (d, *J* = 6.8 Hz, 1H), 7.08–6.97 (m, 1H), 6.88 (d, *J* = 3.6 Hz, 1H), 6.68–6.37 (m, 1H), 4.27–4.11 (m, 2H), 4.10–4.01 (m, 1H), 3.96 (s, 3H), 3.93–3.87 (m, 1H), 3.79–3.68 (m, 3H), 3.37–3.26 (m, 2H), 2.93–2.71 (m, 6H), 2.19–1.93 (m, 9H). LCMS *m/z* (M + H) 510.

1-[3-[7-(difluoromethyl)-6-(1-methylpyrazol-4-yl)-3,4-dihydro-2*H*-quinolin-1-yl]-1-(1-methyl-4-piperidyl)-6,7-dihydro-4*H*-pyrazolo[4,3-*c*]pyridin-5-yl]ethanone (13**). To a solution of 1-(3-(7-(difluoromethyl)-6-(1-methyl-1*H*-pyrazol-4-yl)-3,4-dihydroquinolin-1(2*H*)-yl)-1-(piperidin-4-yl)-6,7-dihydro-1*H*-pyrazolo[4,3-*c*]pyridin-5(4*H*)-yl)ethanone (**12**, 80 mg, 0.16 mmol) in DCE (2 mL) was added sodium cyanoborohydride (30 mg, 0.47 mmol), AcOH (0.05 mL, 0.9 mmol), and formaldehyde (37% in water, 0.035 mL, 0.47 mmol). The mixture was stirred at room temperature for 1 h. The reaction was quenched with satd aq NaHCO₃ (10 mL) and extracted with DCM (10 mL \times 3). The combined organic layers were dried over anhydrous**

Na_2SO_4 , filtered, and concentrated in vacuo. The crude residue was purified by reverse phase chromatography (acetonitrile 24–54%/0.05% NH_4OH in water) to give the title compound (**13**, 19 mg, 23%) as a white solid. ^1H NMR (400 MHz, $\text{DMSO}-d_6$) δ 7.73 (s, 1H), 7.48 (s, 1H), 7.08 (s, 1H), 6.92–6.62 (m, 2H), 4.15–4.10 (m, 2H), 4.02–3.94 (m, 1H), 3.85 (s, 3H), 3.72–3.65 (m, 2H), 3.60–3.55 (m, 2H), 2.83–2.71 (m, 6H), 2.18 (s, 3H), 2.05–1.90 (m, 9H), 1.84–1.75 (m, 2H). LCMS m/z (M + H) 524.

1-[4-[5-Acetyl-3-[7-(difluoromethyl)-6-(1-methylpyrazol-4-yl)-3,4-dihydro-2H-quinolin-1-yl]-6,7-dihydro-4H-pyrazolo[4,3-c]pyridin-1-yl]-1-piperidyl]ethanone (14). Step 1: *tert*-Butyl 1-(1-Acetyl(piperidin-4-yl)-3-(7-(difluoromethyl)-6-(1-methyl-1H-pyrazol-4-yl)-3,4-dihydroquinolin-1(2H)-yl)-6,7-dihydro-1H-pyrazolo[4,3-c]pyridine-5(4H)-carboxylate (**61**). To a solution of *tert*-butyl 1-(1-acetyl(piperidin-4-yl)-3-bromo-6,7-dihydro-1H-pyrazolo[4,3-c]pyridine-5(4H)-carboxylate (**30**, 500 mg, 1.20 mmol) in 1,4-dioxane (3 mL) was added 7-(difluoromethyl)-6-(1-methyl-1H-pyrazol-4-yl)-1,2,3,4-tetrahydroquinoline (**53**, 370 mg, 1.40 mmol), *t*-BuONa (562 mg, 5.9 mmol), and dichloro[1,3-bis(2,6-di-3-pentylphenyl)imidazol-2-ylidene](3-chloropyridyl)palladium(II) (93 mg, 0.12 mmol). The mixture was heated to 120 °C for 12 h under a nitrogen atmosphere. After cooling the reaction to room temperature, DCM (50 mL) was added and washed with water (40 mL × 2) and brine (40 mL). The organic layer was dried over anhydrous Na_2SO_4 , filtered, and concentrated in vacuo. The crude residue was purified by silica gel chromatography (DCM/MeOH = 20:1) to give the title compound (**61**, 300 mg, 42%) as a white solid. ^1H NMR (400 MHz, $\text{DMSO}-d_6$) δ 7.75 (s, 1H), 7.49 (s, 1H), 7.10 (s, 1H), 6.79 (s, 1H), 6.78 (t, J = 55.2 Hz, 1H), 4.48–4.41 (m, 1H), 4.39–4.28 (m, 2H), 4.08–3.98 (m, 2H), 3.94–3.90 (m, 1H), 3.86 (s, 3H), 3.61–3.56 (m, 2H), 3.24–3.09 (m, 1H), 2.84–2.74 (m, 4H), 2.74–2.63 (m, 2H), 2.02 (s, 3H), 1.98–1.85 (m, 6H), 1.41–1.37 (m, 9H). LCMS m/z (M + H) 610.

Step 2: 1-(4-(3-(7-(difluoromethyl)-6-(1-methyl-1H-pyrazol-4-yl)-3,4-dihydroquinolin-1(2H)-yl)-4,5,6,7-tetrahydro-1H-pyrazolo[4,3-c]pyridin-1-yl)piperidin-1-yl)ethanone (**63**). To a solution of *tert*-butyl 1-(1-acetyl(piperidin-4-yl)-3-(7-(difluoromethyl)-6-(1-methyl-1H-pyrazol-4-yl)-3,4-dihydroquinolin-1(2H)-yl)-6,7-dihydro-1H-pyrazolo[4,3-c]pyridine-5(4H)-carboxylate (**61**, 300 mg, 0.500 mmol) in DCM (2 mL) was added trifluoroacetic acid (0.4 mL, 5 mmol). The reaction was stirred at room temperature for 1 h and concentrated in vacuo. The crude residue was diluted with DCM (50 mL) and washed with satd aq NaHCO_3 (30 mL × 2) and water (30 mL) and brine (40 mL). The organic layer was dried over anhydrous Na_2SO_4 , filtered, and concentrated in vacuo to give the title compound (**63**, 200 mg, crude) as a white solid that required no further purification. LCMS m/z (M + H) 510.

Step 3: 1-[4-[5-Acetyl-3-[7-(difluoromethyl)-6-(1-methylpyrazol-4-yl)-3,4-dihydro-2H-quinolin-1-yl]-6,7-dihydro-4H-pyrazolo[4,3-c]pyridin-1-yl]-1-piperidyl]ethanone (**14**). To a solution of 1-(4-(3-(7-(difluoromethyl)-6-(1-methyl-1H-pyrazol-4-yl)-3,4-dihydroquinolin-1(2H)-yl)-4,5,6,7-tetrahydro-1H-pyrazolo[4,3-c]pyridin-1-yl)piperidin-1-yl)ethanone (**63**, 100 mg, 0.17 mmol) in DCM (2 mL) at 0 °C was added triethylamine (0.07 mL, 0.5 mmol) and acetic anhydride (0.02 mL, 0.2 mmol). The mixture was stirred at room temperature for 1 h. DCM (50 mL) was added and washed with water (40 mL) and brine (40 mL). The organic layer was dried over anhydrous Na_2SO_4 , filtered, and concentrated in vacuo. The crude residue was purified by Prep-TLC (DCM/MeOH = 20:1) to give the title compound (**14**, 53 mg, 52%) as a white solid. ^1H NMR (400 MHz, $\text{DMSO}-d_6$) δ 7.75 (s, 1H), 7.50 (s, 1H), 7.10 (s, 1H), 6.94–6.64 (m, 2H), 4.46–4.42 (m, 1H), 4.39–4.26 (m, 1H), 4.21–4.08 (m, 2H), 3.93–3.89 (m, 1H), 3.86 (s, 3H), 3.79–3.65 (m, 2H), 3.63–3.52 (m, 2H), 3.25–3.11 (m, 1H), 2.90–2.83 (m, 3H), 2.80–2.64 (m, 2H), 2.08–1.96 (m, 6H), 1.95–1.83 (m, 5H), 1.80–1.67 (m, 1H). LCMS m/z (M + H) 552.

1-[3-[7-(Difluoromethyl)-6-(1-methylpyrazol-4-yl)-3,4-dihydro-2H-quinolin-1-yl]-1-(1,1-dioxothian-4-yl)-6,7-dihydro-4H-pyrazolo[4,3-c]pyridin-5-yl]ethanone (16). In a similar manner to **14**, compound **16** was prepared from *tert*-butyl 3-bromo-1-(1,1-dioxotetrahydro-2H-thiopyran-4-yl)-6,7-dihydro-1H-pyrazolo[4,3-c]pyridine-5(4H)-carboxylate (**35**) to provide the title compound (**16**, 40%) as a white solid. ^1H NMR (400 MHz, $\text{DMSO}-d_6$) δ 7.76 (s, 1H),

7.50 (s, 1H), 7.11 (s, 1H), 6.94–6.65 (m, 2H), 4.52–4.48 (m, 1H), 4.16–4.11 (m, 2H), 3.86 (s, 3H), 3.75–3.69 (m, 2H), 3.60–3.58 (m, 2H), 3.35–3.30 (m, 2H), 3.25–3.22 (m, 2H), 2.84–2.73 (m, 4H), 2.43–2.41 (m, 2H), 2.23–2.20 (m, 2H), 2.07–1.96 (m, 5H). LCMS m/z (M + H) 559.

3-[7-(Difluoromethyl)-6-(1-methylpyrazol-4-yl)-3,4-dihydro-2H-quinolin-1-yl]-1-tetrahydropyran-4-yl-6,7-dihydro-4H-pyrazolo[4,3-c]pyridine-5-carboxamide (18). Step 1: *tert*-Butyl 3-(7-(difluoromethyl)-6-(1-methyl-1H-pyrazol-4-yl)-3,4-dihydroquinolin-1(2H)-yl)-1-(tetrahydro-2H-pyran-4-yl)-6,7-dihydro-1H-pyrazolo[4,3-c]pyridine-5(4H)-carboxylate (**65**). To a solution of 7-(difluoromethyl)-6-(1-methyl-1H-pyrazol-4-yl)-1,2,3,4-tetrahydroquinoline (**53**, 3.41 g, 13 mmol) in dioxane (100 mL) was added *tert*-butyl 3-bromo-1-(tetrahydro-2H-pyran-4-yl)-6,7-dihydro-1H-pyrazolo[4,3-c]pyridine-5(4H)-carboxylate (**29**, 5.0 g, 12.9 mmol), chloro(2-dicyclohexylphosphino-2',6'-di-i-propoxy-1,1'-biphenyl)[2-(2-aminoethylphenyl)]palladium(II), methyl-*tert*-butylether adduct (1.01 g, 1.30 mmol), 2-dicyclohexylphosphino-2',6'-di-i-propoxy-1,1'-biphenyl (0.60 g, 1.3 mmol), and *t*-BuONa (3.70 g, 38.8 mmol). The mixture was heated to 120 °C for 16 h under an argon atmosphere. After cooling the reaction to room temperature, the mixture was concentrated in vacuo. The crude residue was purified by silica gel chromatography (DCM/MeOH = 100:1) to give the title compound (**65**, 5.4 g, 73%) as a light-yellow solid. LCMS m/z (M + H) 569.

Step 2: 7-(difluoromethyl)-6-(1-methyl-1H-pyrazol-4-yl)-1-(1-(tetrahydro-2H-pyran-4-yl)-4,5,6,7-tetrahydro-1H-pyrazolo[4,3-c]pyridin-3-yl)-1,2,3,4-tetrahydroquinoline (**66**). To a solution of *tert*-butyl 3-(7-(difluoromethyl)-6-(1-methyl-1H-pyrazol-4-yl)-3,4-dihydroquinolin-1(2H)-yl)-1-(tetrahydro-2H-pyran-4-yl)-6,7-dihydro-1H-pyrazolo[4,3-c]pyridine-5(4H)-carboxylate (**65**, 6.3 g, 11 mmol) in DCM (20 mL) was added trifluoroacetic acid (20 mL). The mixture was stirred at 30 °C for 3 h. The reaction was concentrated in vacuo to give the title compound (**66**, 10.8 g, crude) as brown oil which was used to the next step without further purification. LCMS m/z (M + H) 469.

Step 3: 3-[7-(Difluoromethyl)-6-(1-methylpyrazol-4-yl)-3,4-dihydro-2H-quinolin-1-yl]-1-tetrahydropyran-4-yl-6,7-dihydro-4H-pyrazolo[4,3-c]pyridine-5-carboxamide (**18**). To a solution of 7-(difluoromethyl)-6-(1-methylpyrazol-4-yl)-1-(1-tetrahydropyran-4-yl)-4,5,6,7-tetrahydropyrazolo[4,3-c]pyridin-3-yl)-3,4-dihydro-2H-quinoline (**66**, 200 mg, 0.430 mmol) in DCM (2 mL) was added trimethylsilyl isocyanate (0.12 mL, 0.85 mmol). The mixture was stirred at room temperature for 3 h and concentrated in vacuo. The crude residue was purified by reverse phase chromatography (acetonitrile 18–48%/0.1% NH_4OH in water) to give the title compound (**18**, 44 mg, 20%) as a white solid. ^1H NMR (400 MHz, $\text{DMSO}-d_6$) δ 7.75 (s, 1H), 7.50 (s, 1H), 7.09 (s, 1H), 6.83 (s, 1H), 6.78 (t, J = 55.2 Hz, 1H), 6.08 (s, 2H), 4.31–4.26 (m, 1H), 4.02 (s, 2H), 3.97–3.94 (m, 2H), 3.86 (s, 3H), 3.60–3.55 (m, 4H), 3.48–3.42 (m, 2H), 2.84–2.67 (m, 4H), 2.00–1.94 (m, 4H), 1.83–1.80 (m, 2H). LCMS m/z (M + H) 512.

3-[7-(Difluoromethyl)-6-(1-methylpyrazol-4-yl)-3,4-dihydro-2H-quinolin-1-yl]-N-methyl-1-tetrahydropyran-4-yl-6,7-dihydro-4H-pyrazolo[4,3-c]pyridine-5-carboxamide (19). To a solution of 7-(difluoromethyl)-6-(1-methylpyrazol-4-yl)-1-(1-tetrahydropyran-4-yl)-4,5,6,7-tetrahydropyrazolo[4,3-c]pyridin-3-yl)-3,4-dihydro-2H-quinoline (**66**, 10.8 g, 23.0 mmol) and triethylamine (8.1 g, 80 mmol) in DCM (20 mL) was added *N*-methylimidazole-1-carboxamide (4.0 g, 32 mmol). The reaction was stirred at 25 °C for 36 h. Water (20 mL) was added and extracted with DCM (20 mL × 3). The combined organic layers were dried over anhydrous Na_2SO_4 , filtered, and concentrated in vacuo. The crude residue was purified by silica gel chromatography (DCM/MeOH = 100:1) to give the title compound (**19**, 2.7 g, 22%) as a light-yellow solid. ^1H NMR (400 MHz, $\text{DMSO}-d_6$) δ 7.76–7.75 (m, 1H), 7.49 (s, 1H), 7.10 (s, 1H), 6.83 (s, 1H), 6.92–6.78 (t, J = 55.2 Hz, 1H), 6.65–6.53 (m, 1H), 4.31–4.28 (m, 1H), 4.13–3.93 (m, 4H), 3.86 (s, 3H), 3.69–3.58 (m, 4H), 3.48–3.42 (m, 2H), 2.84–2.74 (m, 4H), 2.54–2.53 (m, 3H), 1.97–1.80 (m, 6H). ^{13}C NMR (101 MHz, $\text{DMSO}-d_6$) δ 158.3, 148.0, 142.5, 138.2, 137.9, 131.0, 129.7, 128.9 (t, J = 20.5 Hz), 126.0, 121.0 (t, J = 5.1 Hz), 119.0, 114.2 (t, J = 235.8 Hz), 110.2 (t, J = 6.1 Hz), 106.8, 66.5, 54.0, 49.4, 40.8, 40.7, 39.0, 32.8, 27.6, 27.4, 22.1, 21.9. HRMS m/z 526.2718 (M + H $^+$, $\text{C}_{27}\text{H}_{34}\text{F}_2\text{N}_7\text{O}_2$, requires 526.2742).

3-[7-(Difluoromethyl)-6-(1-methylpyrazol-4-yl)-3,4-dihydro-2H-quinolin-1-yl]-N-ethyl-1-tetrahydropyran-4-yl-6,7-dihydro-4H-pyrazolo[4,3-c]pyridine-5-carboxamide (20). To a solution of pyridine (0.37 mL, 4.6 mmol) and 7-(difluoromethyl)-6-(1-methylpyrazol-4-yl)-1-(tetrahydropyran-4-yl)-4,5,6,7-tetrahydropyrazolo[4,3-c]pyridin-3-yl)-3,4-dihydro-2H-quinoline (66, 362 mg, 0.770 mmol) in DMF (5 mL) was added 4-nitrophenyl chloroformate (467 mg, 2.32 mmol). The reaction was stirred at room temperature for 2 h. Ethanamine (12 mL, 24 mmol) was added to the reaction mixture. The reation was heated to 80 °C for 12 h in a sealed tube. After cooling to room temperature, the reaction mixture was concentrated in vacuo. The crude residue was purified by reverse phase chromatography (acetonitrile 33–51%/0.2% formic acid in water) to give the title compound (20, 57 mg, 14%) as a white solid. ¹H NMR (400 MHz, DMSO-*d*₆) δ 7.75 (s, 1H), 7.49 (s, 1H), 7.09 (s, 1H), 6.83 (s, 1H), 6.78 (t, *J* = 55.6 Hz, 1H), 6.60 (t, *J* = 5.6 Hz, 1H), 4.37–4.20 (m, 1H), 4.01 (s, 2H), 4.00–3.91 (m, 2H), 3.86 (s, 3H), 3.66–3.56 (m, 4H), 3.51–3.39 (m, 2H), 3.02 (q, *J* = 6.8 Hz, 2H), 2.88–2.82 (m, 2H), 2.77–2.72 (m, 2H), 2.07–1.89 (m, 4H), 1.86–1.78 (m, 2H), 0.97 (t, *J* = 6.8 Hz, 3H). LCMS *m/z* (M + H) 540.

3-[7-(Difluoromethyl)-6-(1-methylpyrazol-4-yl)-3,4-dihydro-2H-quinolin-1-yl]-N,N-dimethyl-1-tetrahydropyran-4-yl-6,7-dihydro-4H-pyrazolo[4,3-c]pyridine-5-carboxamide (21). To a solution of triethylamine (0.31 mL, 2.3 mmol) and 7-(difluoromethyl)-6-(1-methylpyrazol-4-yl)-1-(tetrahydropyran-4-yl)-4,5,6,7-tetrahydropyrazolo[4,3-c]pyridin-3-yl)-3,4-dihydro-2H-quinoline (66, 211 mg, 0.450 mmol) in DMF (2 mL) was added dimethylcarbamyl chloride (0.04 mL, 0.45 mmol). The reaction was stirred at room temperature for 16 h. EtOAc (5 mL) was added and washed with water (5 mL). The organic layer was concentrated in vacuo. The crude residue was purified by reverse phase chromatography (acetonitrile 30–60%/0.2% formic acid in water) to give the title compound (21, 55 mg, 22%) as a white solid. ¹H NMR (400 MHz, DMSO-*d*₆) δ 7.76 (s, 1H), 7.50 (s, 1H), 7.10 (s, 1H), 6.81 (s, 1H), 6.79 (t, *J* = 55.2 Hz, 1H), 4.38–4.20 (m, 1H), 4.02–3.90 (m, 2H), 3.87 (s, 3H), 3.84–3.79 (m, 2H), 3.62–3.54 (m, 2H), 3.49–3.42 (m, 2H), 3.41–3.36 (m, 2H), 2.91–2.79 (m, 4H), 2.70 (s, 6H), 2.05–1.91 (m, 4H), 1.88–1.76 (m, 2H). LCMS *m/z* (M + H) 540.

Modeling Methods. All crystal structure figures were made using PyMOL Molecular Graphics System, version 1.8, Schrödinger, LLC.

Expression and Purification of Bromodomain Proteins. The expression and purification of bromodomain proteins was carried out as previously described.^{11,32}

Expression and Purification of Bromodomain Proteins for Crystallography. The expression and purification of CRBP and BRD4 bromodomains for crystallography have been previously described.¹⁴

Time-Resolved Fluorescence Resonance Energy Transfer Assays. Compound potencies were evaluated in a panel of biochemical bromodomain binding assays. Binding of biotinylated small-molecule ligands to recombinant His-tagged bromodomains was assessed by time-resolved fluorescence resonance energy transfer (TR-FRET). Test compounds that compete with the biotinylated ligand for bromodomain binding reduce the TR-FRET signal. All biochemical assay protocols were carried out as previously described.^{11,32,33}

Cellular Assay Protocols. The CBP BRET assay was carried out as previously described.¹¹ To determine the inhibition of MYC expression, MV-4-11 cells (ATCC) were plated at 10000 cells per well in 96-well plates in RPMI1640 media supplemented with 10% fetal bovine serum and 2 mM L-glutamine. Test compounds diluted in DMSO were transferred to the cell plates, keeping final DMSO concentration consistent at 0.1%, and incubated for 4 h at 37 °C. Lysis and analysis for MYC expression were carried out using QuantiGene 2.0 reagents (Affymetrix/eBioscience, probe set cat. no. SA-50182) and following the vendor's instructions. Luminescence was read using an EnVision plate reader (PerkinElmer) and EC₅₀s generated in XLFit using a four-parameter nonlinear regression fit.

In Vitro Metabolic Stability Experiments, MDCK Permeability Experiments, Protein Binding Experiments, and CYP Inhibition Assessment. Experiments were carried out as previously described.¹²

In Vivo PK of 10 and 19. Mouse PK: Twelve female CD-1 mice were obtained from Vital River Laboratory Animal Co., Ltd., Beijing, P.R.

China. All animals were 6–9 weeks old at the time of study and weighed between 20 and 35 g. Animals (*n* = 3 per dosing route) were dosed with 10 or 19 at 1 mg/kg iv (in propyl ethylene glycol 400 (35% v/v) and water (65% v/v)) or 5 mg/kg po (suspended in 0.5% w/v methylcellulose, 0.2% w/v Tween 80). Food and water were available ad libitum to all animals. Serial blood samples (15 μL) were collected by tail nick at 0.033, 0.083, 0.25, 0.5, 1, 3, 8, and 24 h after the intravenous administration and 0.083, 0.25, 0.5, 1, 3, 8, and 24 h after the oral administration. All blood samples were diluted with 60 μL of water containing 1.7 mg/mL EDTA and kept at –80 °C until analysis.

Rat PK: Twelve male Sprague–Dawley rats were obtained from Shanghai SLAC Laboratory Animal Co. Ltd., Shanghai, P.R. China. All animals were 6–9 weeks old at the time of study and weighed between 200 and 300 g. Animals (*n* = 3 per dosing route) were dosed with 10 or 19 at 1 mg/kg iv (in propyl ethylene glycol 400 (35% v/v) and water (65% v/v)) or 5 mg/kg po (suspended in 0.5% w/v methylcellulose, 0.2% w/v Tween 80). Food and water were available ad libitum to animals in the iv groups. Animals in po groups were fasted overnight and food withheld until 4 h postdose. Approximately 250 μL of blood were collected via the catheter at 0.033, 0.083, 0.25, 0.5, 1, 2, 4, 8, and 24 h after the intravenous or oral administration. All blood samples were collected into tubes containing 5 μL of 0.5 M K₂EDTA and processed for plasma. Samples were centrifuged (2500g for 15 min at 4 °C) within 1 h of collection, and plasma samples were kept at –80 °C until analysis.

Dog PK: Twelve non-naïve male beagle dogs were obtained from Marshall Bioresources, Beijing, P.R. China. All animals were 6 months to 2 years old at the time of study and weighed between 6 and 10 kg. Animals (*n* = 3 per dosing route) were dosed with 10 or 19 at 1 mg/kg iv (in ethanol (20% v/v), propyl ethylene glycol 400 (15% v/v) and water (65% v/v)) or 5 mg/kg po (suspended in 0.5% w/v methylcellulose, 0.2% w/v Tween 80). Food and water were available ad libitum to animals in the iv groups. Animals in po groups were fasted overnight and food withheld until 4 h postdose. Approximately 800 μL of blood was collected from a peripheral vessel at predose, 0.033, 0.083, 0.25, 0.5, 1, 3, 6, 9, and 24 h after the intravenous administration and predose, 0.083, 0.25, 0.5, 1, 3, 6, 9, and 24 h after the oral administration. All blood samples were collected into tubes containing 10 μL of 0.5 M K₂EDTA and processed for plasma. Samples were centrifuged (3000g for 10 min at 4 °C) within 1 h of collection, and plasma samples were kept at –80 °C until analysis.

Monkey PK: Twelve non-naïve male cynomolgus monkeys were obtained from Hainan Jingang Laboratory Animal Co. Ltd., Haikou Hainan Province, P.R. China. All animals were at least 2 years old at the time of study and weighed between 2 and 5 kg. Animals (*n* = 3 per dosing route) were dosed with 10 or 19 1 mg/kg iv (in ethanol (20% v/v), propyl ethylene glycol 400 (15% v/v) and water (65% v/v)) or 5 mg/kg po (suspended in 0.5% w/v methylcellulose, 0.2% w/v Tween 80). Food and water were available ad libitum to animals in the iv groups. Animals in po groups were fasted overnight and food withheld until 4 h postdose. Approximately 800 μL of blood was collected from a peripheral vessel at predose, 0.033, 0.083, 0.25, 0.5, 1, 3, 6, 9, and 24 h after the intravenous administration and predose, 0.083, 0.25, 0.5, 1, 3, 6, 9, and 24 h after the oral administration. All blood samples were collected into tubes containing 10 μL of 0.5 M K₂EDTA and processed for plasma. Samples were centrifuged (3000g for 10 min at 4 °C) within 1 h of collection, and plasma samples were kept at –80 °C until analysis.

Bio-analytical method of PK samples: Concentrations of 10 and 19 were determined by a nonvalidated LC-MS/MS assay. The diluted blood samples were prepared for analysis by placing a 25 μL aliquot into a 96-well plate followed by the addition of 200 μL of acetonitrile containing an internal standard mixture (0.1 μg/mL indomethacin). The samples were vortexed and centrifuged at 4000 rpm for 10 min at 4 °C; 50 μL of the supernatant was diluted with 150 μL of water, and 10 μL of the solution was injected onto an analytical column. An Acuity UPLC system (Waters) coupled with an API 4000 mass spectrometer (AB Sciex, Foster City, CA) was used for sample analysis. The mobile phases were 0.025% FA and 1 mM NH₄OAc in water/ACN (v:v, 95:5) (A) and 0.025% FA and 1 mM NH₄OAc in ACN/water (v:v, 95:5) (B). The gradient was as follows: starting at 10% B and increased to 65% B for 1.2 min, then to 95% for 0.6 min, maintained at 95% B for 0.2 min,

then decreased to 10% B within 0.01 min. The total flow rate was 0.6 mL/min, and samples were injected onto an ACE 3 AQ (2.1 mm × 100 mm, 3 μm) analytical column with a total run time of 2 min. Data were acquired using multiple reactions monitoring (MRM) in positive ion electrospray mode with an operating source temperature of 550 °C. The MRM transition was *m/z* 511.400 → 471.400 for **10**, 526.400 → 486.400 for **19**, and 357.900 → 139.000 for indomethacin. The lower and upper limits of quantitation of the assay for **10** were 0.002 and 13.1 μM, respectively. The lower and upper limits of quantitation of the assay for **19** were 0.002 and 12.7 μM, respectively.

In Vivo Evaluation of **19 in MOLM-16 AML PK/PD and Antitumor Efficacy Model.** RT-PCR was performed using TaqMan RNA-to-Ct 1-Step Kit and Taqman Gene Expression Assays (Applied Biosystems, Carlsbad, CA, USA). The comparative Ct method was used to estimate relative changes in gene expression using MYC Taqman assay (Hs00153408_m1) and ACTB TaqMan assay (Hs01060665_g1) as housekeeping gene.

All procedures were approved by and conformed to the guidelines and principles set by the Institutional Animal Care and Use Committee of Genentech and were carried out in an Association for the Assessment and Accreditation of Laboratory Animal Care (AAALAC)-accredited facility. Female C.B-17 SCID/bg mice that were 8–9 weeks old and weighed 20–24 g were obtained from Charles River Lab. They were inoculated with five million MOLM-16 leukemia acute myelogenous cells (suspended in a 1:1 mixture of Hank's Balanced Salt Solution containing Matrigel at a 1:1 ratio) in the right flank subcutaneously. Tumors were monitored until they reached a mean tumor volume of 130–300 mm³. The mean tumor volume across all eight groups was 260 ± 34.5 mm³ (mean ± SD) at the initiation of dosing. Mice were given 0 (vehicle—0.5% methylcellulose, 0.2% Tween-80), 3, 10, and 30 mg/kg of compound **19** by gavage, twice daily (BID) for 21 days in a volume of 100 μL. Tumor volumes were measured in two dimensions (length and width) using Ultra Cal-IV calipers (model S4-10-111; Fred V. Fowler Co., Newton, MA) and analyzed using Excel, version 11.2 (Microsoft Corporation; Redmond WA). The tumor volume was calculated with the following formula: tumor size (mm³) = (longer measurement × shorter measurement²) × 0.5. Animal body weights were measured using an Adventura Pro AV812 scale (Ohaus Corporation; Pine Brook, NJ). Percent weight change was calculated using the following formula: group percent weight change = (new weight – initial weight)/initial weight) × 100. Plasma, tumor, and brain samples were collected at 2 h postdose. To analyze the repeated measurement of tumor volumes from the same animals over time, a mixed-modeling approach was used. This approach addresses both repeated measurements and modest dropouts due to any nontreatment related removal of animals before the end of study. Cubic regression splines were used to fit a nonlinear profile to the time courses of log 2 tumor volume at each dose level. The nonlinear profiles were then related to dose within the mixed model. Tumor growth inhibition as a percentage of vehicle was calculated as the percentage of the area under the fitted tumor volume–time curve (AUC) per day for each dose group in relation to the vehicle, using the following formula: %TGI = 100 × [1 – (AUC_{dose} per day/AUC_{vehicle} per day)].

Concentrations of **19** were determined by a nonvalidated LC-MS/MS assay. The plasma samples were prepared for analysis by placing a 25 μL aliquot into a 96-well plate. The tumor samples were collected and weighed. Four volume of water by tissue weight was added. Using a bead beating homogenizer, the tissue samples were homogenized and 25 μL of each was aliquoted into a 96-well plate. A volume of 200 μL of acetonitrile containing an internal standard (labetalol) was added to the sample. The samples were vortexed and centrifuged at 4000 rpm for 10 min, and 50 μL of the supernatant was diluted with 150 μL of water. A 10 μL injection volume was used for analysis on a SIL-30ACMP autosampler system (Shimadzu, Columbia, MD) was linked to LC-30AD pumps (Shimadzu), coupled with an API 5500 QTrap mass spectrometer (Sciex, Foster City, CA), was used for sample analysis. The mobile phases were 0.1% FA (formic acid) in water (A) and 0.1% FA in MeCN (B). The gradient was as following: starting at 10% B and increased to 90% B in 0.6 min, maintained at 90% B for 0.2 min, then decreased to 10% B within 0.1 min. The total flow rate was 1.2 mL/min

and column for separation was Kinetex XB-C18 column (50 mm × 2.1 mm, 2.6 μm) with a total run time of 1 min. Data were acquired using multiple reactions monitoring (MRM) in positive ion electrospray mode with an operating source temperature of 550 °C. The MRM transition was *m/z* 526.1 → 486.2 for **19** and 329.076 → 294.1 for labetalol. The lower and upper limits of quantitation of the assay for **19** were 0.002 and 39 μM, respectively.

In Vitro Evaluation of **19 on *T_{reg}*.** Human naïve CD4+T cells were isolated from PBMCs of healthy donors using naïve CD4+T Cell Isolation Kit II (Miltenyi Biotec) and differentiated to *iT_{reg}* for 4 days using plate-bound anti-CD3 (5 μg/mL; eBioscience), soluble anti-CD28 (3 μg/mL; eBioscience), plus rTGFβ (5 ng/mL; R&D Systems), and rIL-2 (10 ng/mL; R&D Systems) in complete RPMI-1640 medium (10% FCS, 50 μM 2-mercaptoethanol, 10% penicillin/streptomycin, 10% NEAA, 10% sodium pyruvate). Compound **19** was used at 2 μM and titrated down at 2× dilution. This study followed the principles of research ethics as set forth in the Belmont Report and was approved by the Western Institutional Review Board (WIRB-Protocol number CEHS-CP 3072).

iT_{reg} were stained using antibodies against surface markers CD4 FITC (clone OKT-4) and CD25 Pacific Blue (clone BC96) (all from eBioscience), fixed/permeabilized with the Foxp3/Transcription Factor Staining Buffer Set (eBioscience), and labeled for intracellular Foxp3 APC (clone 259D/C7; BD Biosciences). *iT_{reg}* were stained for viability using fixable viability dye eFluor 781. Samples were acquired on a BD LSR Fortessa using FACSDiva software (BD Biosciences). Data were analyzed using the FlowJo software (TreeStar, FLOWJO, LLC).

Total RNA was isolated from *iT_{reg}* using RNeasy (Qiagen), including an on-column DNase I digestion. cDNA was prepared using High Capacity cDNA Reverse Transcriptase Kit (Life Technologies). Quantitative RT-PCR was performed to determine Foxp3 gene expression levels with the ABI 7900 HT Fast Real-Time PCR System (Applied Biosystems). Gene expression data was normalized to B2M as a housekeeping gene.

Kinetic Solubility Assay. Kinetic solubility assay started with compound DMSO stock solutions. This assay used Millipore Multi-screen 96-well filter plates for the 24 h equilibration shaking. For routine equilibrium solubility determination of discovery chemistry compounds, samples were prepared by adding 4 μL of the 10 mM DMSO stock solution into 196 μL of PBS buffer pH 7.4 in the 96-well filter plates, yielding a compound concentration of 200 μM and 2% DMSO. The PBS buffer pH 7.4 was prepared by the Genentech media lab. The filter plate was sealed with aluminum sealing film and shaken at room temperature for 24 h at 1000 rpm. When shaking was completed, the solutions were filtered into a clean 96-well plate utilizing a vacuum manifold. After filtration, some precipitate was often observed at the bottom of the filtration plate wells. The filtrate samples were diluted by a factor of 2 using PBS pH 7.4 buffer and then transferred to a 384-well plate for analysis by LCMS-CLND (CLND: chemiluminescence nitrogen detector). Then 5 μL of each sample were injected twice into the LCMS-CLND instrument for repeat analysis. Samples were detected and analyzed using UV 254 nm and CLND. UV 254 nm was used primarily to confirm the sample purity but in rare cases was also used to quantify the concentration of compounds with no nitrogen, where additional work was done to create a compound specific calibration curve. The identification of CLND target peaks of each compound was confirmed by LCMS. Sample quantification was accomplished by CLND peak intensity, the CLND calibration curve, and the number of nitrogens contained in the compound. One calibration curve of caffeine was used for solubility quantitative determination. A fresh calibration curve was generated for every batch.

ASSOCIATED CONTENT

S Supporting Information

The Supporting Information is available free of charge on the ACS Publications website at DOI: [10.1021/acs.jmedchem.7b00796](https://doi.org/10.1021/acs.jmedchem.7b00796).

Full experimental details and characterization for all reported compounds, BromoScan data for **10** and **19**,

Cerep off-target screening data for **19**, Invitrogen kinase data for **19**, ab initio torsion scan data for **8**, PK/PD data for **19**, crystallography methods for 3-CBP, 8-CBP, 17-CBP, 10-CBP, 19-CBP, and 19-BRD4(1) (PDF)
Molecular formula strings (CSV)

Accession Codes

PDB codes for the structures of the CBP bromodomain in complex with **3**, **8**, **17**, **10**, and **19** are SW0F, SW0I, SW0L, SW0Q, and SW0E, respectively. PDB code for the structure of the BRD4(1) in complex with **19** is SVZS. Authors will release the atomic coordinates and experimental data upon article publication.

AUTHOR INFORMATION

Corresponding Authors

*For F.A.R. phone, (858) 349-6055; E-mail, anthony.romero@unitybiotechnology.com.

*For S.M. E-mail, magnuson.steven@gene.com.

ORCID®

F. Anthony Romero: 0000-0001-7917-1459

Edna F. Choo: 0000-0003-4200-8302

Terry D. Crawford: 0000-0003-4663-4116

Patrick Cyr: 0000-0001-5320-3483

Stefan G. Koenig: 0000-0002-1878-614X

Notes

The authors declare no competing financial interest.

ACKNOWLEDGMENTS

We thank Suzanne Brown, Ning Liu, Mika Kosaka, Emile Plise, and Jonathan Cheong in the DMPK department and Mengling Wong, Michael Hayes, and Amber Guillen for compound purification. Baiwei Lin, Deven Wang, and Yutao Jiang are acknowledged for analytical support. Grady Howes, Jan Seerveld, Hao Zheng, and Gigi Yuen for help with compound management and logistics are also recognized. This research used resources of the Advanced Light Source, which is a DOE Office of Science User Facility under contract no. DE-AC02-05CH11231. We would like to acknowledge the beamline staff at ALS 5.0.2 for their help and support.

ABBREVIATIONS USED

AML, acute myeloid leukemia; BAZ2B, bromodomain adjacent to zinc finger domain 2B; BET, bromodomain and extra terminal; Boc, *tert*-butyloxycarbonyl; BPTF, bromodomain plant homeodomain finger transcription factor; BRD4(X), bromodomain X (X = 1, 2) of the bromodomain-containing protein 4; BRD8, bromodomain-containing protein 8; BRD9, bromodomain-containing protein 9; BRET, bioluminescence resonance energy transfer; BRPF1, bromodomain and plant homeodomain finger containing 1; CBP, cyclic adenosine monophosphate response element binding protein, binding protein; CECR2, cat eye syndrome chromosome region, candidate 2; Cl_{hep}, predicted hepatic clearance; CNS, central nervous system; DBU, 1,8-diazabicyclo[5.4.0]undec-7-ene; DCE, dichloroethane; DCM, dichloromethane; DIEA, *N,N*-diisopropylethyl amine; DMF, *N,N*-dimethylformamide; DMSO, dimethyl sulfoxide; DNA, deoxyribonucleic acid; Foxp3, forkhead box P3; GCNSL, general control of amino-acid synthesis 5-like 2; HAT, histone acetyl transferase; HATU, 1-[bis(dimethylamino)methylene]-1*H*-1,2,3-triazolo[4,5-*b*]-pyridinium 3-oxide hexafluorophosphate; iv, intravenous; KAc,

acetylated lysine; *K*_{p_{uu}}, ratio of the unbound drug concentration in brain to unbound drug concentration in plasma; LE, ligand efficiency; LLE, lipophilic ligand efficiency; LM, liver microsomes; MeCN, acetonitrile; NBS, *N*-bromosuccinimide; po, per os; P300, adenoviral E1A binding protein; *P*_{app} A–B, apparent permeability apical-to-basolateral; PBMCs, peripheral blood mononuclear cells; PCAF, P300/CBP-associated factor; PK, pharmacokinetic; QD, one a day; q-RT-PCR, quantitative reverse transcriptase polymerase chain reaction; SAR, structure–activity relationship; SEM, [2-(trimethylsilyl)ethoxy]-methyl; SFC, supercritical fluid chromatography;; TAF1(X), bromodomain X (X = 1, 2) of the TATA-box binding protein associated factor 1; TEA, triethylamine; TFA, trifluoroacetic acid; THF, tetrahydrofuran; THP, tetrahydropyran; THQ, tetrahydroquinoline; tPSA, total polar surface area; TR-FRET, time-resolved fluorescence energy transfer

REFERENCES

- (1) Bannister, A. J.; Kouzarides, T. The CBP Co-Activator Is a Histone Acetyltransferase. *Nature* **1996**, *384*, 641–643.
- (2) Delvecchio, M.; Gaucher, J.; Aguilar-Gurrieri, C.; Ortega, E.; Panne, D. Structure of the P300 Catalytic Core and Implications for Chromatin Targeting and HAT Regulation. *Nat. Struct. Mol. Biol.* **2013**, *20*, 1040–1046.
- (3) Mujtaba, S.; He, Y.; Zeng, L.; Yan, S.; Plotnikova, O.; Sachchidanand, Sanchez, R.; Zeleznik-Le, N. J.; Ronai, Z.; Zhou, M.-M. Structural Mechanism of the Bromodomain of the Coactivator CBP in P53 Transcriptional Activation. *Mol. Mol. Cell* **2004**, *13*, 251–263.
- (4) Iyer, N. G.; Ozdag, H.; Caldas, C. p300/CBP and Cancer. *Oncogene* **2004**, *23*, 4225–4231.
- (5) Dutta, R.; Tiu, B.; Sakamoto, K. M. CBP/P300 Acetyltransferase Activity in Hematologic Malignancies. *Mol. Genet. Metab.* **2016**, *119*, 37–43.
- (6) Dekker, F. J.; Haisma, H. J. Histone Acetyl Transferases as Emerging Drug Targets. *Drug Discovery Today* **2009**, *14*, 942–948.
- (7) Fujisawa, T.; Filippakopoulos, P. Functions of Bromodomain-Containing Proteins and Their Roles in Homeostasis and Cancer. *Nat. Rev. Mol. Cell Biol.* **2017**, *18*, 246–262.
- (8) Liu, Y.; Wang, L.; Predina, J.; Han, R.; Beier, U. H.; Wang, L.-C. S.; Kapoor, V.; Bhatti, T. R.; Akimova, T.; Singhal, S.; Brindle, P. K.; Cole, P. A.; Albelda, S. M.; Hancock, W. W. Inhibition of P300 Impairs Foxp3+ T Regulatory Cell Function and Promotes Antitumor Immunity. *Nat. Med.* **2013**, *19*, 1173–1177.
- (9) Conery, A. R.; Centore, R. C.; Neiss, A.; Keller, P. J.; Joshi, S.; Spillane, K. L.; Sandy, P.; Hatton, C.; Pardo, E.; Zawadzke, L.; Bommi-Reddy, A.; Gascoigne, K. E.; Bryant, B. M.; Mertz, J. A.; Sims, R. J. Bromodomain Inhibition of the Transcriptional Coactivators CBP/EP300 as a Therapeutic Strategy to Target the IRF4 Network in Multiple Myeloma. *eLife* **2016**, *5*, 10483.
- (10) Ghosh, S.; Taylor, A.; Chin, M.; Huang, H.-R.; Conery, A. R.; Mertz, J. A.; Salmeron, A.; Dakle, P. J.; Mele, D.; Côté, A.; Jayaram, H.; Setser, J. W.; Poy, F.; Hatzivassiliou, G.; DeAlmeida-Nagata, D.; Sandy, P.; Hatton, C.; Romero, F. A.; Chiang, E.; Reimer, T.; Crawford, T.; Pardo, E.; Watson, V. G.; Tsui, V.; Cochran, A. G.; Zawadzke, L.; Harmange, J.-C.; Audia, J. E.; Bryant, B. M.; Cummings, R. T.; Magnuson, S. R.; Grogan, J. L.; Bellon, S. F.; Albrecht, B. K.; Sims, R. J., III; Lora, J. M. Regulatory T Cell Modulation by CBP/EP300 Bromodomain Inhibition. *J. Biol. Chem.* **2016**, *291*, 13014–13027.
- (11) Taylor, A. M.; Côté, A.; Hewitt, M. C.; Pastor, R.; Leblanc, Y.; Nasveschuk, C. G.; Romero, F. A.; Crawford, T. D.; Cantone, N.; Jayaram, H.; Setser, J.; Murray, J.; Beresini, M. H.; de Leon Boenig, G.; Chen, Z.; Conery, A. R.; Cummings, R. T.; Dakin, L. A.; Flynn, E. M.; Huang, O. W.; Kaufman, S.; Keller, P. J.; Kiefer, J. R.; Lai, T.; Li, Y.; Liao, J.; Liu, W.; Lu, H.; Pardo, E.; Tsui, V.; Wang, J.; Wang, Y.; Xu, Z.; Yan, F.; Yu, D.; Zawadzke, L.; Zhu, X.; Zhu, X.; Sims, R. J., III; Cochran, A. G.; Bellon, S.; Audia, J. E.; Magnuson, S.; Albrecht, B. K. Fragment-Based Discovery of a Selective and Cell-Active Benzodiazepine CBP/EP300

- Bromodomain Inhibitor (CPI-637). *ACS Med. Chem. Lett.* **2016**, *7*, 531–536.
- (12) Crawford, T. D.; Romero, F. A.; Lai, K. W.; Tsui, V.; Taylor, A. M.; de Leon Boenig, G.; Noland, C. L.; Murray, J.; Ly, J.; Choo, E. F.; Hunsaker, T. L.; Chan, E. W.; Merchant, M.; Kharbanda, S.; Gascoigne, K. E.; Kaufman, S.; Beresini, M. H.; Liao, J.; Liu, W.; Chen, K. X.; Chen, Z.; Conery, A. R.; Côté, A.; Jayaram, H.; Jiang, Y.; Kiefer, J. R.; Kleinheinz, T.; Li, Y.; Maher, J.; Pardo, E.; Poy, F.; Spillane, K. L.; Wang, F.; Wang, J.; Wei, X.; Xu, Z.; Xu, Z.; Yen, I.; Zawadzke, L.; Zhu, X.; Bellon, S.; Cummings, R.; Cochran, A. G.; Albrecht, B. K.; Magnuson, S. Discovery of a Potent and Selective in Vivo Probe (GNE-272) for the Bromodomains of CBP/EP300. *J. Med. Chem.* **2016**, *59*, 10549–10563.
- (13) Popp, T. A.; Tallant, C.; Rogers, C.; Fedorov, O.; Brennan, P. E.; Müller, S.; Knapp, S.; Bracher, F. Development of Selective CBP/P300 Benzoxazepine Bromodomain Inhibitors. *J. Med. Chem.* **2016**, *59*, 8889–8912.
- (14) Rooney, T. P. C.; Filippakopoulos, P.; Fedorov, O.; Picaud, S.; Cortopassi, W. A.; Hay, D. A.; Martin, S.; Tumber, A.; Rogers, C. M.; Philpott, M.; Wang, M.; Thompson, A. L.; Heightman, T. D.; Pryde, D. C.; Cook, A.; Paton, R. S.; Müller, S.; Knapp, S.; Brennan, P. E.; Conway, S. J. A Series of Potent CREBBP Bromodomain Ligands Reveals an Induced-Fit Pocket Stabilized by a Cation-II Interaction. *Angew. Chem., Int. Ed.* **2014**, *53*, 6126–6130.
- (15) Hay, D. A.; Fedorov, O.; Martin, S.; Singleton, D. C.; Tallant, C.; Wells, C.; Picaud, S.; Philpott, M.; Monteiro, O. P.; Rogers, C. M.; Conway, S. J.; Rooney, T. P. C.; Tumber, A.; Yapp, C.; Filippakopoulos, P.; Bunnage, M. E.; Müller, S.; Knapp, S.; Schofield, C. J.; Brennan, P. E. Discovery and Optimization of Small-Molecule Ligands for the CBP/P300 Bromodomains. *J. Am. Chem. Soc.* **2014**, *136*, 9308–9319.
- (16) Unzue, A.; Xu, M.; Dong, J.; Wiedmer, L.; Spiliotopoulos, D.; Caflisch, A.; Nevado, C. Fragment-Based Design of Selective Nanomolar Ligands of the CREBBP Bromodomain. *J. Med. Chem.* **2016**, *59*, 1350–1356.
- (17) Picaud, S.; Fedorov, O.; Thanasiopoulos, A.; Leonards, K.; Jones, K.; Meier, J.; Olzschka, H.; Monteiro, O.; Martin, S.; Philpott, M.; Tumber, A.; Filippakopoulos, P.; Yapp, C.; Wells, C.; Che, K. H.; Bannister, A.; Robson, S.; Kumar, U.; Parr, N.; Lee, K.; Lugo, D.; Jeffrey, P.; Taylor, S.; Vecellio, M. L.; Bountra, C.; Brennan, P. E.; O'Mahony, A.; Velichko, S.; Müller, S.; Hay, D.; Daniels, D. L.; Urh, M.; La Thangue, N. B.; Kouzarides, T.; Prinjha, R.; Schwaller, J.; Knapp, S. Generation of a Selective Small Molecule Inhibitor of the CBP/P300 Bromodomain for Leukemia Therapy. *Cancer Res.* **2015**, *75*, 5106–5119.
- (18) Hammitsch, A.; Tallant, C.; Fedorov, O.; O'Mahony, A.; Brennan, P. E.; Hay, D. A.; Martinez, F. O.; Al-Mossawi, M. H.; de Wit, J.; Vecellio, M.; Wells, C.; Wordsworth, P.; Müller, S.; Knapp, S.; Bowness, P. CBP30, a Selective CBP/P300 Bromodomain Inhibitor, Suppresses Human Th17 Responses. *Proc. Natl. Acad. Sci. U. S. A.* **2015**, *112*, 10768–10773.
- (19) Denny, R. A.; Flick, A. C.; Coe, J. W.; Langille, J.; Basak, A.; Liu, S.; Stock, I. A.; Sahasrabudhe, P.; Bonin, P. D.; Hay, D. A.; Brennan, P. E.; Pletcher, M. T.; Jones, L. H.; Chekler, E. L. P. Structure-Based Design of Highly Selective Inhibitors of the CREB Binding Protein Bromodomain. *J. Med. Chem.* **2017**, *60*, 5349–5363.
- (20) Romero, F. A.; Magnuson, S.; Pastor, R.; Tsui, V.; Murray, J.; Crawford, T.; Albrecht, B. K.; Côté, A.; Taylor, A. M.; Lai, K. W.; Chen, K. X.; Bronner, S.; Adler, M.; Egen, J.; Liao, J.; Wang, F.; Cyr, P.; Zhu, B.-Y.; Kauder, S. 4,5,6,7-Tetrahydro-1*H*-pyrazolo[4,3-C]pyridin-3-amine Compounds as CBP and/or EP300 Inhibitors. WO2016086200. 2016.
- (21) Romero, F. A.; Taylor, A. M.; Crawford, T. D.; Tsui, V.; Côté, A.; Magnuson, S. Disrupting Acetyl-Lysine Recognition: Progress in the Development of Bromodomain Inhibitors. *J. Med. Chem.* **2016**, *59*, 1271–1298.
- (22) The (*S*) absolute stereochemistry of **8** was determined from the cocrystal structure of **8** in the CBP bromodomain. In every instance the (*S*)-enantiomer was always more potent than the (*R*)-enantiomer (data not shown). Compounds **3**, **5**, **6**, **7**, and **9** were synthesized from (*R*)-tetrahydrofuran-3-ol and thus the absolute stereochemistry is unambiguously that of the (*S*)-configuration.
- (23) Mo Ka Molecular Discovery, Perugia. <http://www.moldiscovery.com/software/moka/> (Accessed July 27, 2017).
- (24) Leeson, P. D.; Springthorpe, B. The Influence of Drug-Like Concepts on Decision-Making in Medicinal Chemistry. *Nat. Rev. Drug Discovery* **2007**, *6*, 881–890.
- (25) Hopkins, A. L.; Groom, C. R.; Alex, A. Ligand Efficiency: A Useful Metric for Lead Selection. *Drug Discovery Today* **2004**, *9*, 430–431.
- (26) Chan, H. M.; La Thangue, N. B. P300/CBP Proteins: HATs for Transcriptional Bridges and Scaffolds. *J. Cell Sci.* **2001**, *114*, 2363–2373.
- (27) Sakaguchi, S.; Yamaguchi, T.; Nomura, T.; Ono, M. Regulatory T Cells and Immune Tolerance. *Cell* **2008**, *133*, 775–787.
- (28) Tanaka, A.; Sakaguchi, S. Regulatory T Cells in Cancer Immunotherapy. *Cell Res.* **2017**, *27*, 109–118.
- (29) Shimizu, J.; Yamazaki, S.; Sakaguchi, S. Induction of Tumor Immunity by Removing CD25+ CD4+ T Cells: a Common Basis Between Tumor Immunity and Autoimmunity. *J. Immunol.* **1999**, *163*, 5211–5218.
- (30) Hori, S.; Nomura, T.; Sakaguchi, S. Control of Regulatory T Cell Development by the Transcription Factor Foxp3. *Science* **2003**, *299*, 1057–1061.
- (31) Liu, Y.; Wang, L.; Han, R.; Beier, U. H.; Akimova, T.; Bhatti, T.; Xiao, H.; Cole, P. A.; Brindle, P. K.; Hancock, W. W. Two Histone/Protein Acetyltransferases, CBP and P300, Are Indispensable for Foxp3+ T-Regulatory Cell Development and Function. *Mol. Cell. Biol.* **2014**, *34*, 3993–4007.
- (32) Crawford, T. D.; Tsui, V.; Flynn, E. M.; Wang, S.; Taylor, A. M.; Côté, A.; Audia, J. E.; Beresini, M. H.; Burdick, D. J.; Cummings, R. T.; Dakin, L. A.; Duplessis, M.; Good, A. C.; Hewitt, M. C.; Huang, H.-R.; Jayaram, H.; Kiefer, J. R.; Jiang, Y.; Murray, J. M.; Nasveschuk, C. G.; Pardo, E.; Poy, F.; Romero, F. A.; Tang, Y.; Wang, J.; Xu, Z.; Zawadzke, L. E.; Zhu, X.; Albrecht, B. K.; Magnuson, S. R.; Bellon, S. F.; Cochran, A. G. Diving Into the Water: Inducible Binding Conformations for BRD4, TAF1(2), BRD9, and CECR2 Bromodomains. *J. Med. Chem.* **2016**, *59*, 5391–5402.
- (33) Albrecht, B. K.; Gehling, V. S.; Hewitt, M. C.; Vaswani, R. G.; Côté, A.; Leblanc, Y.; Nasveschuk, C. G.; Bellon, S.; Bergeron, L.; Campbell, R.; Cantone, N.; Cooper, M. R.; Cummings, R. T.; Jayaram, H.; Joshi, S.; Mertz, J. A.; Neiss, A.; Normant, E.; O'Meara, M.; Pardo, E.; Poy, F.; Sandy, P.; Supko, J.; Sims, R. J., III; Harmange, J.-C.; Taylor, A. M.; Audia, J. E. Identification of a Benzoisoxazoloazepine Inhibitor (CPI-0610) of the Bromodomain and Extra-Terminal (BET) Family as a Candidate for Human Clinical Trials. *J. Med. Chem.* **2016**, *59*, 1330–1339.